

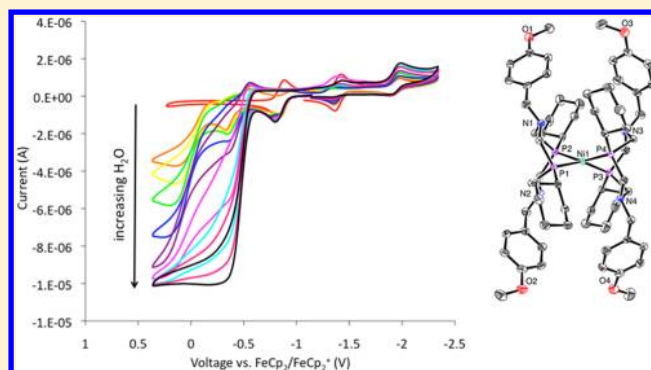
Incorporating Amino Acid Esters into Catalysts for Hydrogen Oxidation: Steric and Electronic Effects and the Role of Water as a Base

Sheri Lense, Ming-Hsun Ho, Shentan Chen, Avijita Jain,[†] Simone Raugei, John C. Linehan, John A. S. Roberts, Aaron M. Appel, and Wendy Shaw*

Pacific Northwest National Laboratory, Richland, Washington 99354, United States

Supporting Information

ABSTRACT: Four derivatives of a hydrogen oxidation catalyst, $[\text{Ni}(\text{P}^{\text{Cy}}_2\text{N}^{\text{Bn-R}})_2]^{2+}$ (Cy = cyclohexyl, Bn = benzyl, R = OMe, COOMe, CO-alanine-methyl ester, CO-phenyl-alanine-methyl ester), have been prepared to investigate steric and electronic effects on catalysis. Each complex was characterized spectroscopically and electrochemically, and thermodynamic data were determined. Crystal structures are also reported for the -OMe and -COOMe derivatives. All four catalysts were found to be active for H_2 oxidation. The methyl ester (R = COOMe) and amino acid ester containing complexes (R = CO-alanine-methyl ester or CO-phenyl-alanine-methyl ester) had rates slower (4 s^{-1}) than that of the parent complex (10 s^{-1}), in which R = H, which is consistent with the lower amine pK_a 's and less favorable ΔG_{H_2} 's found for these electron-withdrawing substituents. Dynamic processes for the amino acid ester containing complexes were also investigated and found not to hinder catalysis. The electron-donating methyl ether derivative (R = OMe) was prepared to compare electronic effects and has a catalytic rate similar to that of the parent complex. In the course of these studies, it was found that water could act as a weak base for H_2 oxidation, although catalytic turnover requires a higher potential and utilizes a different sequence of catalytic steps than when using a base with a higher pK_a . Importantly, these catalysts provide a foundation upon which larger peptides can be attached to $[\text{Ni}(\text{P}^{\text{Cy}}_2\text{N}^{\text{Bn}})_2]^{2+}$ hydrogen oxidation catalysts in order to more fully investigate and implement the effects of the outer coordination sphere.



Dynamic processes for the amino acid ester containing complexes were also investigated and found not to hinder catalysis. The electron-donating methyl ether derivative (R = OMe) was prepared to compare electronic effects and has a catalytic rate similar to that of the parent complex. In the course of these studies, it was found that water could act as a weak base for H_2 oxidation, although catalytic turnover requires a higher potential and utilizes a different sequence of catalytic steps than when using a base with a higher pK_a . Importantly, these catalysts provide a foundation upon which larger peptides can be attached to $[\text{Ni}(\text{P}^{\text{Cy}}_2\text{N}^{\text{Bn}})_2]^{2+}$ hydrogen oxidation catalysts in order to more fully investigate and implement the effects of the outer coordination sphere.

INTRODUCTION

Hydrogenases catalyze the production or oxidation of hydrogen, reactions which are of widespread interest for the production and utilization of renewable fuels. Using abundant metals, Ni and/or Fe, hydrogenases catalyze this reaction with high rates and low overpotentials.^{1–3} Catalysis at the hydrogenase active site is enhanced by the surrounding protein scaffold, including the second coordination sphere (amino acids which interact with but do not bind to the metal) and the outer coordination sphere (OCS) (amino acids which do not interact with the metal). The stable secondary and tertiary structures of the outer coordination sphere are thought to be vital to enhancing catalysis by stabilizing the active site, controlling the environment around the active site and mediating the transfer of H_2 , protons, and electrons between the buried active site and the exterior of the protein.^{1,4–7}

Many structural and functional synthetic analogues of hydrogenases have been made.^{8,9} The family of $[\text{Ni}(\text{P}^{\text{R}}_2\text{N}^{\text{R}'})_2]^{2+}$ complexes (Scheme 1) mimics the second coordination sphere of $[\text{FeFe}]$ -hydrogenases by including a positioned pendant amine, resulting in rate enhancements of several orders of magnitude in comparison to catalysts without

a positioned amine.^{8,10} The R and R' substituents can be varied to tune the catalysts for H_2 production (Scheme 1, counter-clockwise) or oxidation (Scheme 1, clockwise).^{10–13} In addition to the species implicated in the catalytic cycle, two noncatalytically active isomers (endo-exo and exo-exo)^{14,15} of the diprotonated tetrahedral $\text{Ni}(0)$ product are observed which have important consequences for catalysis.^{12,16} In more recent derivatives, these catalysts meet or exceed the rates of the enzymes,^{15,17} but at higher overpotentials. The combination of high catalytic rates and low overpotentials, characteristic of hydrogenases, is still not being achieved with catalyst biomimics, indicating that the outer coordination sphere in the enzyme plays an important role in achieving fast rates at low overpotentials.

Effects of the second and outer coordination spheres on molecular catalysts were assessed for hydrogen production catalysts by attaching amino acids, amino acid esters, and dipeptides to a derivative of the $[\text{Ni}(\text{P}^{\text{Ph}}_2\text{N}^{\text{Ph-R}})_2]^{2+}$ proton reduction catalyst.¹⁸ The resulting catalytic rates ranged over an

Received: May 14, 2012

Published: September 24, 2012



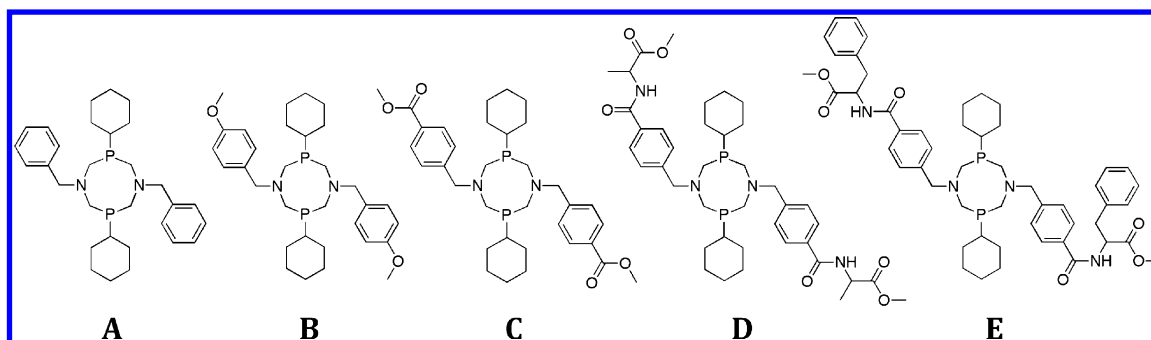
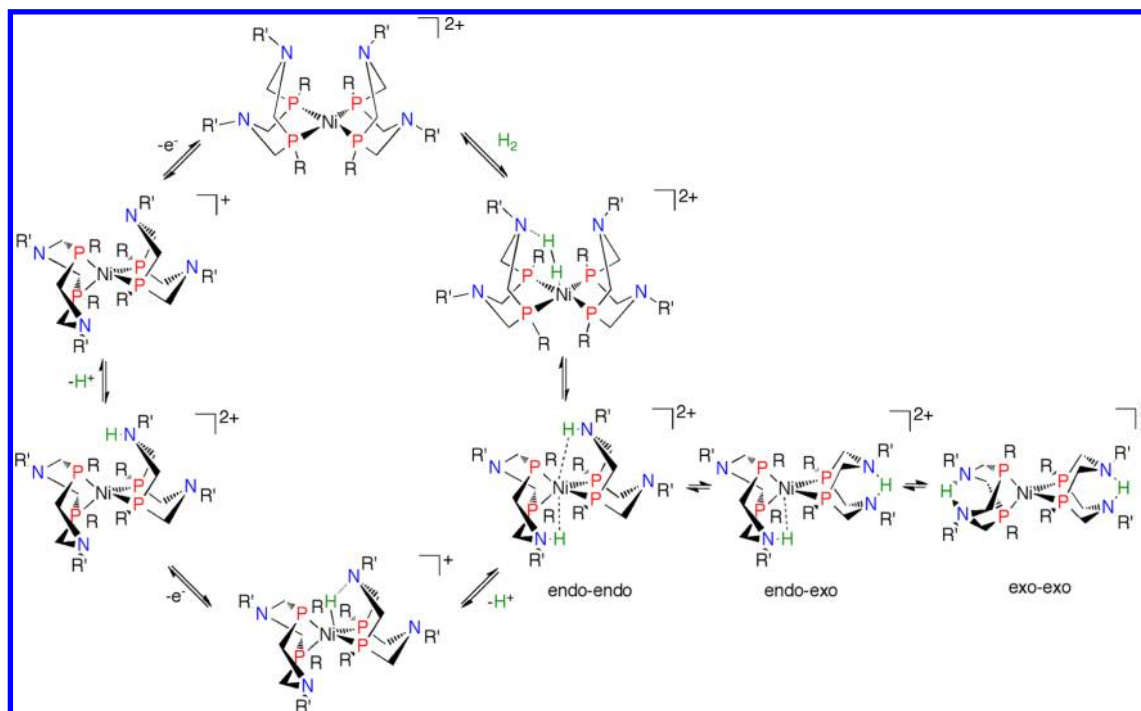
Scheme 1. Mechanism for H₂ Production (Counterclockwise) and Oxidation (Clockwise) by [Ni(P^R₂N^{R'}₂)₂]²⁺ Complexes

Figure 1. Ligands used in this study to make Ni(P^{Cy}₂N^{Bn-R})₂ complexes are derivatives of P^{Cy}₂N^{Bn} (A), including P^{Cy}₂N^{Bn-OMe} (B), P^{Cy}₂N^{Bn-COOMe} (C), P^{Cy}₂N^{Bn-Ala-OMe} (D), and P^{Cy}₂N^{Bn-Phe-OMe} (E).

order of magnitude, demonstrating the ability of the outer coordination sphere to modulate the catalytic activity of a molecular catalyst, despite the remoteness from the metal center. Separate studies assessed the effect of para substituents with varying electron-donating ability on [Ni(P^{Ph}₂N^{Ph-R})₂]²⁺ and found a significant dependence of the catalytic rate on the R substituents, despite their distance from the metal, due to their effect on the pendant amine pK_a.¹⁷

While several different effects of the second and outer coordination sphere (amine pK_a and amino acid functionality) on hydrogen production catalysts have been reported,^{17,18} their impact on hydrogen oxidation catalysts has been relatively unexplored. In this work, we investigate the role of the second and outer coordination spheres by modifying the groups on the pendant amines of hydrogen oxidation catalysts, [Ni(P^{Cy}₂N^{Bn})₂]²⁺, using ether, ester, and amino acid ester derivatives. The ligands for these catalysts are shown in Figure 1. To investigate electronic effects, the methyl ester (C) and the similar methyl ether derivative (B) were incorporated into the catalyst. Nonpolar ester-protected amino acid containing complexes were also prepared by coupling the amino acid esters alanine (Ala) and phenylalanine (Phe) to the hydrolyzed

methyl ester derivative (D and E), enabling the study of steric effects in the absence of additional functional groups. The full characterization of these new complexes is presented, and insight into how these groups alter the thermodynamics and catalytic activity of the parent complex is provided.

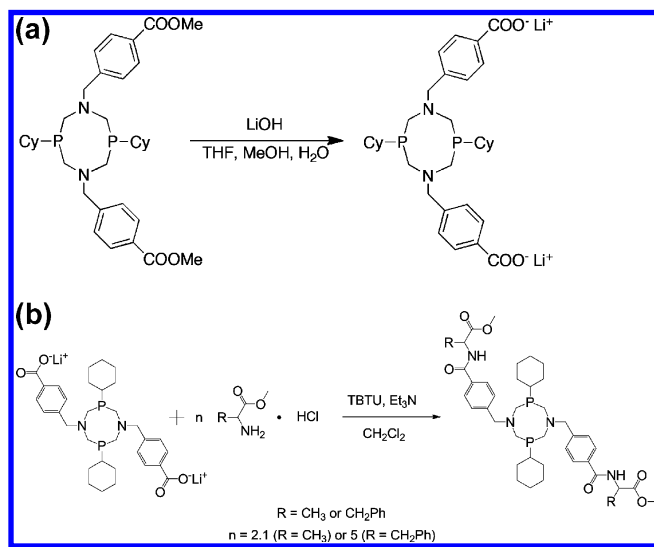
RESULTS AND DISCUSSION

Synthesis and Characterization of Ligands and Metal

Complexes. The P^R₂N^{R'}₂ ligands were synthesized by heating bis(hydroxymethylcyclohexyl)phosphine and the appropriate amine or ammonium hydrochloride salt precursor in ethanol, as described previously.¹⁰ The ligands were characterized by mass spectrometry and ³¹P{¹H} and ¹H NMR spectroscopy, resulting in data that are consistent with the proposed structures and with previous complexes of this type.^{10,18} The ligand P^{Cy}₂N^{Bn-OMe} (1B) could not be synthesized cleanly or purified by recrystallization; therefore, the impure ligand was metallated to form [Ni^{II}(P^{Cy}₂N^{Bn-OMe})₂](BF₄)₂ and then reduced to [Ni⁰(P^{Cy}₂N^{Bn-OMe})₂], which precipitates cleanly from acetonitrile.¹⁹

Amino acid ester complexes were prepared by coupling methyl ester protected amino acid hydrochlorides (alanine (Ala) and phenylalanine (Phe)) to $\text{P}^{\text{Cy}}_2\text{N}^{\text{Bn-COO-Li}^+}_2$ to form the ligands $\text{P}^{\text{Cy}}_2\text{N}^{\text{Bn-Ala-OMe}}_2$ and $\text{P}^{\text{Cy}}_2\text{N}^{\text{Bn-Phe-OMe}}_2$, respectively, using TBTU as the coupling reagent (Scheme 2b and Figure 1D,E).

Scheme 2. Synthesis of (a) $\text{P}^{\text{Cy}}_2\text{N}^{\text{Bn-COO-Li}^+}_2$ and (b) $\text{P}^{\text{Cy}}_2\text{N}^{\text{Bn-R-OMe}}_2$ (R = Ala, Phe)



Attempts to directly synthesize the precursor ligand to which amino acids would be attached, $\text{P}^{\text{Cy}}_2\text{N}^{\text{Bn-COOH}}_2$, were unsuccessful; therefore, this ligand was synthesized by hydrolysis of $\text{P}^{\text{Cy}}_2\text{N}^{\text{Bn-COOMe}}_2$ (Scheme 2a). In addition to the standard characterization, ^1H - ^1H TOCSY NMR spectroscopy was used to identify the amide proton via coupling to the C_α proton and other protons in the side chain (Figure 2 and Figure S1 (Supporting Information)). Integration of the ^1H NMR spectra showed complete coupling of each amino acid ester to $\text{P}^{\text{Cy}}_2\text{N}^{\text{Bn-COO-Li}^+}_2$, in particular through the comparison of the intensity of the amide and C_α protons to the benzyl protons on the amine and methylene protons of the eight-membered P_2N_2 ring. In the case of $\text{P}^{\text{Cy}}_2\text{N}^{\text{Bn-Phe-OMe}}_2$ (**1E**), a large excess (5 equiv) of the amino acid ester was used during coupling to increase the yield, as only $\sim 5\%$ coupling occurred when the amino acid ester was added in slight excess. Attempts to drive the reaction forward by the addition of *N*-hydroxybenzotriazole

(HOBt) resulted in oxidation of the phosphines, and consequently its use was avoided.

The ligands were metallated by stirring with 0.5 equivalents of $[\text{Ni}(\text{CH}_3\text{CN})_6](\text{BF}_4)_2$ in acetonitrile. The complexes were characterized by mass spectrometry, elemental analysis, ^1H and ^{31}P NMR spectroscopy, and, when possible, X-ray crystallography. The data were consistent with previous data reported for similar complexes.¹⁰ $[\text{Ni}(\text{P}^{\text{Cy}}_2\text{N}^{\text{Bn-Ala-OMe}}_2)_2]^{2+}$ and $[\text{Ni}(\text{P}^{\text{Cy}}_2\text{N}^{\text{Bn-Phe-OMe}}_2)_2]^{2+}$ were also characterized by ^1H - ^1H TOCSY NMR.

The Ni(0) complexes were generated by reacting the Ni(II) complexes with hydrogen followed by deprotonation with tetramethylguanidine (TMG). Unfortunately, the Ni(0) complexes of the amino acid ester coupled ligands could not be generated in this way. Following addition of TMG, the complex forms a precipitate shown by NMR spectroscopy to be a complex mixture of products, presumably resulting from deprotonation of the amide, which destabilizes the complex. Attempts to form the amino acid ester containing Ni(0) complexes with a weaker base, triethylamine, only generated the Ni(II) hydride complexes rather than the twice deprotonated Ni(0) complexes.

Structural Characterization: X-ray Crystallography. X-ray-quality crystals of $[\text{Ni}(\text{P}^{\text{Cy}}_2\text{N}^{\text{Bn-COOMe}}_2)](\text{BF}_4)_2$ and $[\text{Ni}(\text{P}^{\text{Cy}}_2\text{N}^{\text{Bn-OMe}}_2)](\text{BF}_4)_2$ were obtained by slow diffusion of ether into acetonitrile solutions of the complexes. As in the parent complex, $[\text{Ni}(\text{P}^{\text{Cy}}_2\text{N}^{\text{Bn}}_2)]^{2+}$,¹⁰ all of the six-membered Ni-P-C-N-C-P chelate rings are in boat configurations. The metal is four-coordinate and displays a distorted square planar geometry. The structures are shown in Figure 3, and the structural parameters are compared to those of the parent complex in Table 1. These show that the addition of electron-withdrawing or -donating substituents to the benzyl group does not alter the first coordination sphere significantly.

The crystal structures of $\text{Ni}^0(\text{P}^{\text{Cy}}_2\text{N}^{\text{Bn-COOMe}}_2)_2$, $\text{Ni}^0(\text{P}^{\text{Cy}}_2\text{N}^{\text{Bn}}_2)_2$ and $\text{Ni}^0(\text{P}^{\text{Cy}}_2\text{N}^{\text{Bn-OMe}}_2)_2$, shown in Figure 4, are similar to each other as well as to other related complexes.^{20,21} In all of these complexes, the Ni is in a pseudotetrahedral geometry and each P_2N_2 ligand contains one chelate ring in a chair configuration and one chelate ring in a boat configuration. Structural parameters are given in Table 2. As was observed for the Ni(II) complexes, the addition of electron-withdrawing or -donating substituents to the benzyl group has a negligible effect on the first coordination sphere of the Ni(0) complexes.

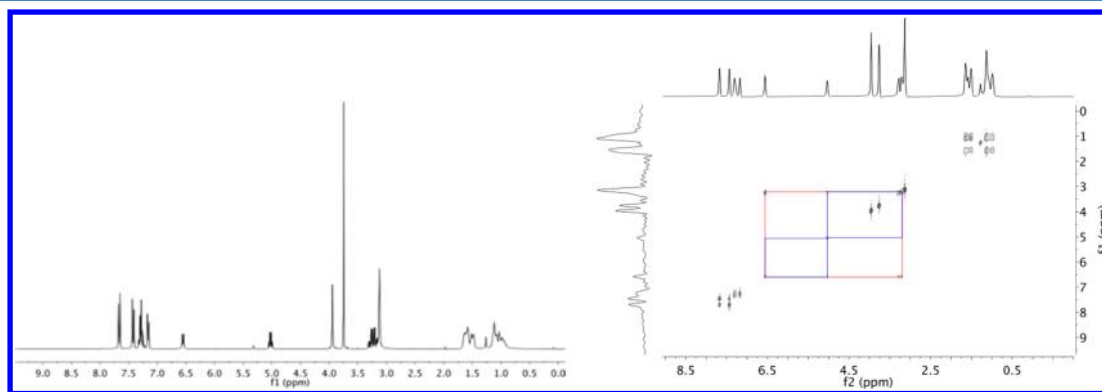


Figure 2. ^1H NMR spectrum (left) and ^1H - ^1H TOCSY spectrum (right) of $\text{P}^{\text{Cy}}_2\text{N}^{\text{Bn-Phe-OMe}}_2$ (**1E**) in CD_2Cl_2 . The blue and red boxes indicate coupling between the amide proton, the C_α proton, and the side chain protons, used to confirm amino acid incorporation.

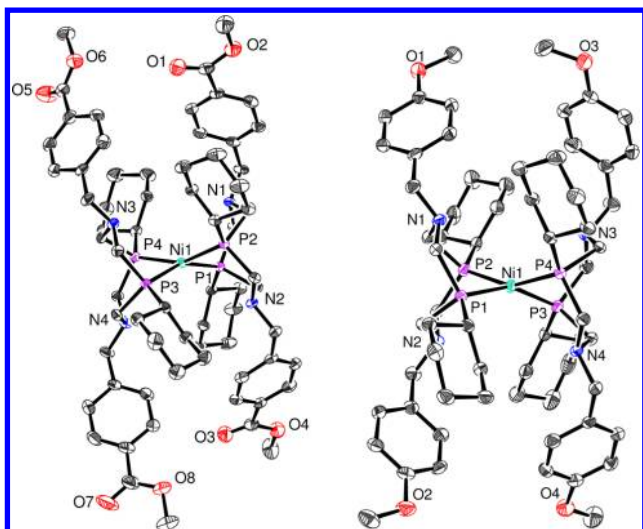


Figure 3. Crystal structures of $[\text{Ni}(\text{P}_2\text{C}_y\text{N}^{\text{Bn-COOMe}}_2)_2](\text{BF}_4)_2$ (left) and $[\text{Ni}(\text{P}_2\text{C}_y\text{N}^{\text{Bn-OMe}}_2)_2](\text{BF}_4)_2$ (right), showing that the active sites of the catalysts are similar despite derivatization of the Bn group. Nickel is shown in green, nitrogen in blue, phosphorus in purple, oxygen in red, and carbon in black. Solvent molecules, counterions, and hydrogen atoms have been omitted for clarity.

NMR Spectroscopy: Structural and Chemical Dynamics in the Amino Ester Derivatives. Addition of the amino acid ester groups to the ligands would be expected to introduce structural rigidity to the metal complexes, due to the steric bulk of the amino acid ester groups and the potential for hydrogen bonding. Indeed, the ^{31}P NMR resonances for $[\text{Ni}(\text{P}^{\text{Cy}}_2\text{N}^{\text{Bn-Ala-OMe}}_2)_2]^{2+}$ and $[\text{Ni}(\text{P}^{\text{Cy}}_2\text{N}^{\text{Bn-Phe-OMe}}_2)_2]^{2+}$ are much broader than those of the other $[\text{Ni}(\text{P}^{\text{Cy}}_2\text{N}^{\text{Bn-R}}_2)_2]^{2+}$ complexes at room temperature (Figure 5). These complexes are thought to be distorted trigonal bipyramidal in solution, with the fifth ligand situated in an equatorial position. The fifth ligand is solvent, an agostic interaction with the electrons in the C–H bond of the benzyl methylene group, or the BF_4^- counterion.^{10,18} An averaged but broad peak is usually observed due to exchange between the axial and equatorial positions for each phosphorus atom. Comparison of the variable-temperature ^{31}P NMR spectroscopy of the amino acid ester derivative $[\text{Ni}(\text{P}^{\text{Cy}}_2\text{N}^{\text{Bn-Ala-OMe}}_2)_2]^{2+}$ and that of the methyl ester derivative $[\text{Ni}(\text{P}^{\text{Cy}}_2\text{N}^{\text{Bn-COOMe}}_2)_2]^{2+}$ show that exchange is slower for the amino acid ester derivative, with coalescence occurring approximately 10 °C higher in temperature (Figure 5). At their coalescence temperatures of approximately 10 and 20 °C, respectively, $[\text{Ni}(\text{P}^{\text{Cy}}_2\text{N}^{\text{Bn-COOMe}}_2)_2]^{2+}$ and $[\text{Ni}(\text{P}^{\text{Cy}}_2\text{N}^{\text{Bn-Ala-OMe}}_2)_2]^{2+}$

$[\text{Ni}(\text{P}^{\text{Cy}}_2\text{N}^{\text{Bn-Ala-OMe}}_2)_2]^{2+}$ have exchange rates of $\sim 15\,000\text{ s}^{-1}$. Therefore, despite the hindered structural dynamics observed for $[\text{Ni}(\text{P}^{\text{Cy}}_2\text{N}^{\text{Bn-Ala-OMe}}_2)_2]^{2+}$, the dynamics are still much faster than catalysis at room temperature (*vide infra*).

H_2 addition requires a correctly positioned pendant amine, with one Ni–P–C–N–C–P ring in the boat configuration,²² and the bulky amino acid ester substituents could hinder the chair-to-boat isomerization process. We are not able to measure this process directly, but measurements of the intramolecular proton exchange rates for the diprotonated isomers of $[\text{Ni}(\text{P}^{\text{Cy}}_2\text{N}^{\text{Bn-R}}_2\text{H}_2)_2]^{2+}$ (Scheme 1) provide a relative measure of the chair-to-boat isomerization, since these isomerizations were found to be the slowest steps in transferring the proton from one amine to the other.²³ To provide a measure of this isomerization process, intramolecular proton transfer in $[\text{Ni}(\text{P}^{\text{Cy}}_2\text{N}^{\text{Bn-Phe-OMe}}_2\text{H}_2)_2]^{2+}$ was compared to that in the parent complex $[\text{Ni}(\text{P}^{\text{Cy}}_2\text{N}^{\text{Bn}}_2\text{H}_2)_2]^{2+}$.

At room temperature, the ^{31}P NMR spectra of these complexes contain a single resonance each for the endo-endo and exo-exo isomers (Scheme 1) and two resonances for the endo-exo isomer (Figure 6).²⁴ As the temperature is decreased, the ^{31}P resonances for the endo-endo and endo-exo species resolve as proton transfer between the amines is slowed.²³ Analyzing the line shape of the ^{31}P resonances as a function of temperature, we determined the activation parameters for proton transfer in the endo-exo isomer of $[\text{Ni}(\text{P}^{\text{Cy}}_2\text{N}^{\text{Bn-Phe-OMe}}_2\text{H}_2)_2]^{2+}$ and compared them to that of $[\text{Ni}(\text{P}^{\text{Cy}}_2\text{N}^{\text{Bn}}_2\text{H}_2)_2]^{2+}$ (Table 3). For $[\text{Ni}(\text{P}^{\text{Cy}}_2\text{N}^{\text{Bn-Phe-OMe}}_2\text{H}_2)_2]^{2+}$, proton transfer is slower and the activation enthalpy and free energy are more positive than for $[\text{Ni}(\text{P}^{\text{Cy}}_2\text{N}^{\text{Bn}}_2\text{H}_2)_2]^{2+}$. The data for the endo-endo isomer of $[\text{Ni}(\text{P}^{\text{Cy}}_2\text{N}^{\text{Bn-Phe-OMe}}_2\text{H}_2)_2]^{2+}$ could not be fit due to a second overlapping exchange process (see below), but it can be seen qualitatively that proton transfer for the endo-endo isomer is also slower than that of the parent complex. The exo-exo isomer was not observed to exchange at any temperature studied. The slower exchange rates observed for the Phe-OMe substituted complex suggest that the chair-to-boat isomerizations are more hindered in the complexes substituted with the bulky amino acid ester ligands. However, despite the reduction in rate, it is still several orders of magnitude faster than catalysis at room temperature (*vide infra*) and should not influence catalytic rates.

Unlike $[\text{Ni}(\text{P}^{\text{Cy}}_2\text{N}^{\text{Bn}}_2\text{H}_2)_2]^{2+}$, which contains only two doublets at $-40\text{ }^\circ\text{C}$ for the endo-endo isomer,^{12,23} $[\text{Ni}(\text{P}^{\text{Cy}}_2\text{N}^{\text{Bn-Phe-OMe}}_2\text{H}_2)_2]^{2+}$ has four doublets at $-40\text{ }^\circ\text{C}$. Additionally, the downfield endo-exo resonance of the parent complex remains a single sharp peak,^{12,23} while that of $[\text{Ni}(\text{P}^{\text{Cy}}_2\text{N}^{\text{Bn-Phe-OMe}}_2\text{H}_2)_2]^{2+}$ splits into two peaks at $-20\text{ }^\circ\text{C}$.

Table 1. Structural Parameters of $[\text{Ni}(\text{P}^{\text{Cy}}_2\text{N}^{\text{Bn-OMe}}_2)_2]^{2+}$, $[\text{Ni}(\text{P}^{\text{Cy}}_2\text{N}^{\text{Bn}}_2)_2]^{2+}$, and $[\text{Ni}(\text{P}^{\text{Cy}}_2\text{N}^{\text{Bn-COOMe}}_2)_2]^{2+}$

	$[\text{Ni}(\text{P}^{\text{Cy}}_2\text{N}^{\text{Bn-OMe}}_2)_2]^{2+}$	$[\text{Ni}(\text{P}^{\text{Cy}}_2\text{N}^{\text{Bn}}_2)_2]^{2+}$ ^a	$[\text{Ni}(\text{P}^{\text{Cy}}_2\text{N}^{\text{Bn-COOMe}}_2)_2]^{2+}$
Ni–P1 (Å)	2.1885(8)	2.2048(13)	2.1828(2)
Ni–P2 (Å)	2.1955(8)	2.2055(14)	2.1891(2)
Ni–P3 (Å)	2.1913(8)		2.1961(1)
Ni–P4 (Å)	2.1850(9)		2.2020(2)
Ni–N(1,2,3,4) (Å)	3.376(2), 3.247(2), 3.283(2), 3.257(2)	3.28(7), 3.28(8), N/A, N/A	3.31, 3.36, 3.27, 3.36
P1–Ni–P2, P3–Ni–P4 (deg)	82.53(3), 82.66(3)	82.74(6), N/A	81.85, 82.57
dihedral angle (deg)	41.42	34.87	40.62
space group	<i>Pbca</i>	<i>C2/c</i>	<i>P2_1/c</i>
R1	0.0579	0.0651	0.0819

^aCrystal structure obtained previously by Wilson et al.¹⁰

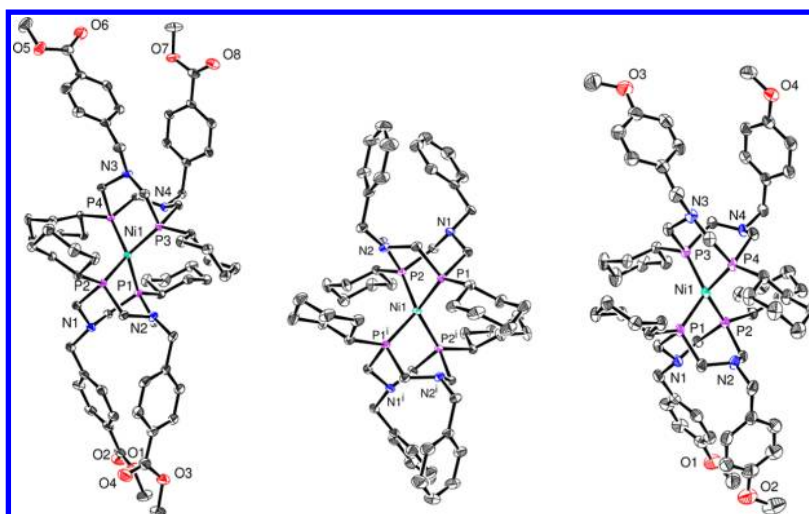


Figure 4. Crystal structures of $\text{Ni}^0(\text{P}(\text{C}_y)_2\text{N}^{\text{Bn-COOMe}}_2)_2$, $\text{Ni}^0(\text{P}(\text{C}_y)_2\text{N}^{\text{Bn}}_2)_2$, and $\text{Ni}^0(\text{P}(\text{C}_y)_2\text{N}^{\text{Bn-OMe}}_2)_2$, demonstrating the similarity between the substituted and unsubstituted $\text{Ni}^0(\text{P}(\text{C}_y)_2\text{N}^{\text{Bn-R}}_2)_2$ derivatives. Nickel is shown in green, nitrogen in blue, phosphorus in purple, oxygen in red, and carbon in black. Hydrogen atoms have been omitted for clarity.

Table 2. Structural Parameters of $[\text{Ni}(\text{P}(\text{C}_y)_2\text{N}^{\text{Bn-OMe}}_2)_2]$, $[\text{Ni}(\text{P}(\text{C}_y)_2\text{N}^{\text{Bn}}_2)_2]$, and $[\text{Ni}(\text{P}(\text{C}_y)_2\text{N}^{\text{Bn-COOMe}}_2)_2]$

	$[\text{Ni}(\text{P}(\text{C}_y)_2\text{N}^{\text{Bn-COOMe}}_2)_2]$	$[\text{Ni}(\text{P}(\text{C}_y)_2\text{N}^{\text{Bn}}_2)_2]$	$[\text{Ni}(\text{P}(\text{C}_y)_2\text{N}^{\text{Bn-OMe}}_2)_2]$
Ni–P1,P2,P3,P4 (Å)	2.1271(8), 2.1268(8), 2.1315(8), 2.1358(8)	2.1376(3), 2.1375(3), 2.1302(3), 2.1301(3)	2.1231(5), 2.1232(5), 2.1261(5), 2.1278(5)
Ni–N1,N2,N3,N4 (Å)	3.783(2) 3.341(3) 3.800(2) 3.415(2)	3.7922(1) 3.3631(1)	3.7697(1), 3.4127(1), 3.7859(1), 3.4003(1)
P1–Ni–P2, P3–Ni–P4 (deg)	86.06(3), 85.43(3)	85.450(9) 85.446(9)	85.854(19), 85.373(19)
dihedral angle (deg)	88.94	88.67	89.09
R1	0.0622	0.0364	0.0507
space group	$\text{P}\bar{1}$	$\text{C}2/c$	$\text{P}\bar{1}$

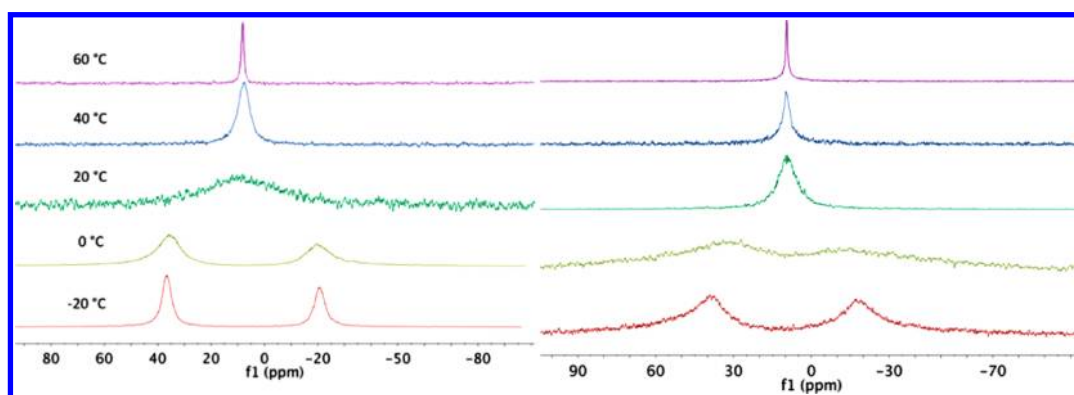


Figure 5. Variable-temperature ^{31}P NMR spectra of $[\text{Ni}(\text{P}(\text{C}_y)_2\text{N}^{\text{Bn-Ala-OMe}}_2)_2]^{2+}$ (left) and $[\text{Ni}(\text{P}(\text{C}_y)_2\text{N}^{\text{COOMe}}_2)_2]^{2+}$ (right) in acetonitrile, showing a slower exchange process for the amino acid ester containing complex.

The parent complex was described as an AA'BB' spin system. The observations for $[\text{Ni}(\text{P}(\text{C}_y)_2\text{N}^{\text{Bn-Phe-OMe}}_2)_2]^{2+}$ are most consistent with an ABMN system, or four unique phosphorus atoms, pairs of which couple to each other. This interpretation is based on the ^{31}P – ^{31}P COSY spectrum at -40 °C, which shows that each doublet couples only to a doublet in the opposite pair (Figure S2 (Supporting Information)). A dependence on field strength (300 and 500 MHz ^1H frequency) was also observed for the difference in frequency between each pair of doublets, whereas the coupling for each doublet was independent of field, confirming that the spectrum for the endo-endo isomer is due to four chemically inequivalent phosphorus atoms (Figure S3 (Supporting Information)).

These results suggest reduced conformational flexibility or a minor structural change in comparison to the parent complex upon protonation.

The resonance belonging to $[\text{HNi}(\text{P}(\text{C}_y)_2\text{N}^{\text{Bn-Phe-OMe}}_2)_2]^+$ also coalesces at temperatures warmer than that observed for the parent complex. Variable temperature NMR spectra of $[\text{HNi}(\text{P}(\text{C}_y)_2\text{N}^{\text{Bn-Phe-OMe}}_2)_2]^+$ in butyronitrile from -80 to $+25$ °C are shown in Figure S4 (Supporting Information). Combined, the structural and proton transfer dynamics suggest reduced freedom and higher energy barrier processes when amino acid esters are incorporated into the outer coordination sphere, but these barriers are not high enough to affect catalysis.

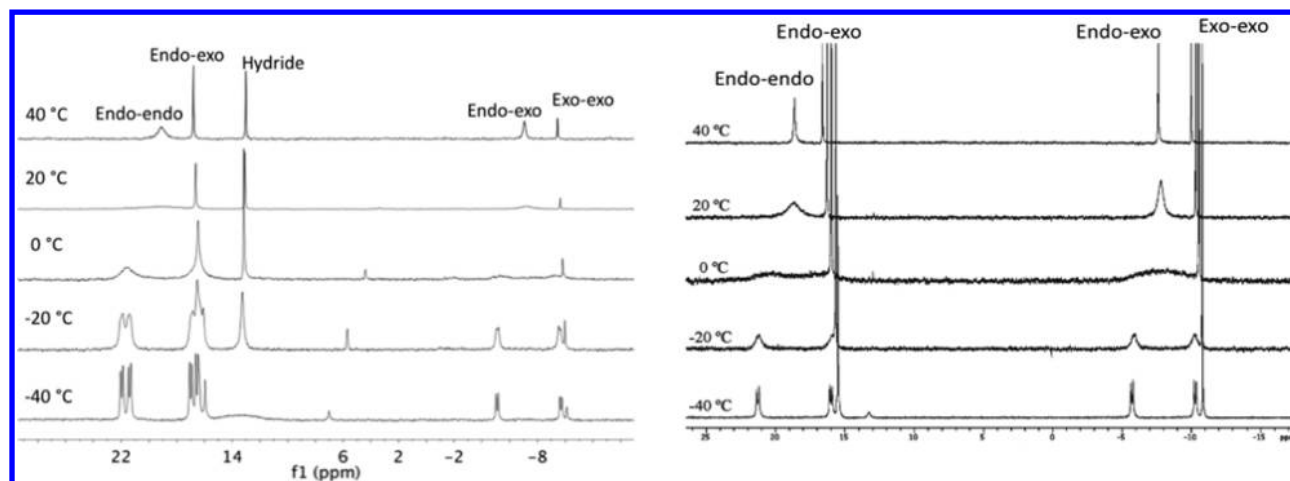


Figure 6. Variable-temperature ^{31}P NMR spectra of $[\text{Ni}(\text{PCy}_2\text{N}^{\text{Bn-Phe-OMe}}_2\text{H})_2]^{2+}$ (left) and $[\text{Ni}(\text{PCy}_2\text{N}^{\text{Bn}}_2\text{H})_2]^{2+}$ (right) in CD_3CN . The figure for $[\text{Ni}(\text{PCy}_2\text{N}^{\text{Bn}}_2\text{H})_2]^{2+}$ was taken from a paper previously published by O'Hagan et al.²³ The spectra for $[\text{Ni}(\text{PCy}_2\text{N}^{\text{Bn-Phe-OMe}}_2\text{H})_2]^{2+}$ show exchange rates slower than those previously observed for $[\text{Ni}(\text{PCy}_2\text{N}^{\text{Bn}}_2\text{H})_2]^{2+}$.

Table 3. Proton Exchange Activation Parameters for the Endo-Exo Isomer of $[\text{Ni}(\text{PCy}_2\text{N}^{\text{Bn-Phe-OMe}}_2\text{H})_2]^{2+}$ and $[\text{Ni}(\text{PCy}_2\text{N}^{\text{Bn}}_2\text{H})_2]^{2+}$ in CD_3CN

	ΔH^\ddagger (kcal/mol)	ΔS^\ddagger (cal/ (mol K))	$\Delta G^\ddagger(298\text{ K})$ (kcal/mol)	$k(298\text{ K})$ (s^{-1}) ^b
R = Bn-Phe-OMe	17.4 ± 0.3	18.1 ± 0.9	12.1 ± 0.3	8700
R = Bn ^a	14.8 ± 0.3	11.4 ± 0.9	11.4 ± 0.3	27000

^aActivation parameters measured previously by O'Hagan et al.²³

^bRates at 298 K are calculated from the activation parameters.

Electrochemistry and Thermodynamic Measurements of the $[\text{Ni}(\text{PCy}_2\text{N}^{\text{Bn-R}}_2)]$ Complexes. Under N_2 , $\text{Ni}(\text{PCy}_2\text{N}^{\text{Bn-COOMe}}_2)_2$ and $\text{Ni}(\text{PCy}_2\text{N}^{\text{Bn-OMe}}_2)_2$ display reversible Ni(II/I) and Ni(I/0) couples in acetonitrile and benzonitrile (Table S1 (Supporting Information)). The potential for the Ni(II/I) redox couple becomes less negative as the electron-donating nature of the benzyl substituent decreases (Table 4). The Ni(I/0) couple is most negative for $\text{Ni}(\text{PCy}_2\text{N}^{\text{Bn-OMe}}_2)_2$ due to the electron-donating group but similar for $\text{Ni}(\text{PCy}_2\text{N}^{\text{Bn-COOMe}}_2)_2$ and $\text{Ni}(\text{PCy}_2\text{N}^{\text{Bn}}_2)_2$. $[\text{Ni}(\text{PCy}_2\text{N}^{\text{Bn-Ala-OMe}}_2)_2]^{2+}$ and $[\text{Ni}(\text{PCy}_2\text{N}^{\text{Bn-Phe-OMe}}_2)_2]^{2+}$ also display reversible Ni(II/I) couples in acetonitrile when the scan is reversed before the Ni(I/0) couple ($\Delta E_p^{\text{II/I}} \approx 78\text{ mV}$). In cyclic voltammograms that scan through both the Ni(II/I) and Ni(I/0) couples, both couples are irreversible due to insolubility of the Ni(0) species in acetonitrile. As expected, the Ni(II/I) couple shifts to more anodic potentials as the substituent becomes more electron withdrawing (Table 4).

For the complexes $[\text{Ni}(\text{PCy}_2\text{N}^{\text{Bn-R}}_2)]$ (R = OMe, COOMe), the pK_a of the pendant amine increases with increased electron-donating character of the benzyl substituent (15.0 and 12.5, respectively), as expected (Table 4). The pK_a values of the pendant amine for $[\text{Ni}(\text{PCy}_2\text{N}^{\text{Bn-Ala-OMe}}_2\text{H})_2]^{2+}$ and $[\text{Ni}(\text{PCy}_2\text{N}^{\text{Bn-Phe-OMe}}_2\text{H})_2]^{2+}$ were found to be 12.8 and 12.5, respectively, similar to that of $[\text{Ni}(\text{PCy}_2\text{N}^{\text{Bn-COOMe}}_2\text{H})_2]^{2+}$. From these values and the potentials of the Ni(II/I) and Ni(I/0) couples, we calculated the ΔG_{H_2} and ΔG_{H^-} values shown in Table 4. The ΔG_{H_2} value was also determined by experimentally measuring the pK_a of the hydride ($[\text{HNi}(\text{PCy}_2\text{N}^{\text{Bn-OMe}}_2)_2]^+$), rather than using the Ni(I/0) couple. The pK_a in benzonitrile was found to be 22.6, yielding a ΔG_{H_2} value of -3.6 kcal/mol , which is in good agreement with the value calculated on the basis of the Ni(I/0) couple (-3.6 kcal/mol). Previous pK_a measurements in acetonitrile and benzonitrile have shown similar values.²⁵ The calculated free energies of hydrogen addition, ΔG_{H_2} , for catalysts containing methyl ester and amino acid ester substituents are less favorable than that of the parent complex, whereas the methyl ether substituted catalyst has a slightly more favorable ΔG_{H_2} .

Cyclic Voltammograms (CV's) of the $[\text{Ni}(\text{PCy}_2\text{N}^{\text{Bn-R}}_2)]$ Complexes under H_2 . Upon sparging solutions of $[\text{Ni}(\text{PCy}_2\text{N}^{\text{Bn-R}}_2)]^+$ (R = COOMe, OMe) with H_2 , the E_p value for the Ni(II/I) oxidation shifts to a slightly more negative potential. The oxidation product, $[\text{Ni}^{\text{II}}(\text{PCy}_2\text{N}^{\text{Bn-R}}_2)_2]^{2+}$, then reacts with H_2 , forming $[\text{Ni}^0(\text{PCy}_2\text{N}^{\text{Bn-R}}_2\text{H})_2]^{2+}$, which isomer-

Table 4. Electrochemical and Thermodynamic Data for Each of the $\text{Ni}(\text{PCy}_2\text{N}^{\text{Bn-R}}_2)_2$ Derivatives^a

complex	$E_{1/2}^{\text{II/I}}$ (V)	$E_{1/2}^{\text{I/0}}$ (V)	TOF(PhCN) (s^{-1})	TOF(MeCN/ H_2O) (s^{-1})	$\text{pK}_a(\text{amine})$	$\text{pK}_a(\text{NiH})$	ΔG_{H_2} (kcal/mol)	ΔG_{H^-} (kcal/mol)
$\text{Ni}(\text{PCy}_2\text{N}^{\text{Bn}}_2)_2$	-0.80^d	-1.28^d	5.6 ± 0.6	$10^d, 9^e$	13.4^d	21.2	-3.1^d	60.7
$\text{Ni}(\text{PCy}_2\text{N}^{\text{Bn-COOMe}}_2)_2$	-0.74	-1.29	4.1 ± 0.4	2.1 ± 0.2^f	12.5	21.3^b	-2.4^b	61.3^b
$\text{Ni}(\text{PCy}_2\text{N}^{\text{Bn-OMe}}_2)_2$	-0.85	-1.39	7.2 ± 1.8	7.1 ± 0.1	15.0	23.2^b	$-3.6^{b,c}$	59.1^b
$[\text{Ni}(\text{PCy}_2\text{N}^{\text{Bn-Ala-OMe}}_2)_2]^{2+}$	-0.78	-1.30	3.9 ± 0.6	3.4 ± 0.1	12.8	21.5^b	-2.3^b	60.8^b
$[\text{Ni}(\text{PCy}_2\text{N}^{\text{Bn-Phe-OMe}}_2)_2]^{2+}$	-0.78	-1.31	2.2 ± 0.5	3.9 ± 0.2	12.5	21.7^b	-1.9^b	60.8^b

^aUnless otherwise noted, all measurements were in acetonitrile. ^bCalculated using equations in the Experimental Section. ^cConfirmed using experimentally measured $\text{pK}_a(\text{NiH})$ in benzonitrile, as described in the Experimental Section. ^dPreviously reported by Wilson et al.¹⁰ ^eRate measured in this study. ^fRate measured at the endo-exo $[\text{Ni}(\text{PCy}_2\text{N}^{\text{Bn-COOMe}}_2\text{H})_2]^{2+}$ oxidation potential.

izes to the endo-endo, endo-exo, and exo-exo isomers (Scheme 1) on the time scale of the CV. The Ni(II/I) oxidation was not seen when $R' = \text{Ala-OMe}$ or $R' = \text{Phe-OMe}$, since it was necessary to start in the $[\text{Ni}^{\text{II}}(\text{P}^{\text{Cy}}_2\text{N}^{\text{Bn-R}}_2)_2]^{2+}$ oxidation state, which immediately reacts with H_2 to form $[\text{Ni}(\text{P}^{\text{Cy}}_2\text{N}^{\text{Bn-R}}_2\text{H})_2]^{2+}$. Each isomer oxidizes irreversibly at a distinct potential at scan rates up to 1 V s^{-1} . CVs for the methyl ether substituted complex, $[\text{Ni}(\text{I})(\text{P}^{\text{Cy}}_2\text{N}^{\text{Bn-OMe}}_2)_2]^+$, illustrative of what is typically observed, are shown in Figure 7.

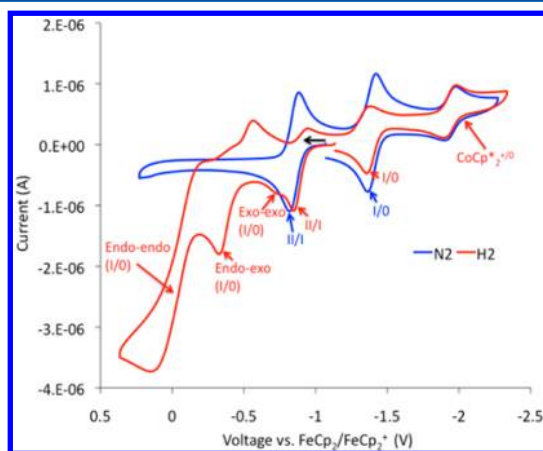


Figure 7. CVs of $[\text{Ni}(\text{P}^{\text{Cy}}_2\text{N}^{\text{Bn-OMe}}_2)_2]^+$ under N_2 (blue trace) and H_2 (red trace), representative of CVs observed for each of the $[\text{Ni}(\text{P}^{\text{Cy}}_2\text{N}^{\text{Bn-R}}_2)_2]$ complexes and showing that each of the three conformational isomers formed upon the addition of H_2 (shown in Scheme 1) have a unique oxidation potential.

Understanding the electrochemistry of each of the isomers may provide mechanistic insight and aid in future catalyst design.¹⁶ Consistent with work by Weidner et al.,¹⁶ the irreversible oxidation events following the Ni(II/I) oxidation can be attributed to redox chemistry of the exo-exo (-0.74 V), endo-exo (-0.33 V) and endo-endo (-0.04 V) isomers of $[\text{Ni}^0(\text{P}^{\text{Cy}}_2\text{N}^{\text{Bn-OMe}}_2\text{H})_2]^{2+}$. Provided that any kinetic potential shifts perturb the oxidation current responses for these isomers in a consistent way, we may assume that the order in the oxidation peak potentials tracks the relative stabilities of the Ni(I) vs Ni(0) states for each of the isomers. The hydrogen bonds between Ni and H–N in the endo configuration (Scheme 1) stabilize the Ni(0) versus the Ni(I) state, resulting in a shift of the Ni(I/0) oxidation to more positive potentials. The potentials for each of the complexes are shown in Table 5. The first Ni...H hydrogen bond results in a shift of 350–410 mV (i.e. the endo-exo isomer), whereas the second Ni...H hydrogen bond (i.e. the endo-endo isomer) results in a shift of 230–290 mV.

The differences in oxidation potentials observed here are larger than those observed for the previously reported complex $[\text{Ni}^0(\text{P}^{\text{tBu}}_2\text{N}^{\text{Bn}}_2\text{H})_2]^{2+}$, wherein the $E_{1/2}$ of the endo-endo isomer was found to be 170 mV positive of the $E_{1/2}$ for the endo-exo isomer, which is 320 mV positive of the $E_{1/2}$ for the exo-exo isomer (Table 5).¹⁶ To understand the origin of the difference in oxidation potentials, DFT calculations were used to compare the Ni...H–N hydrogen-bonding distances for the endo-endo isomers of $[\text{Ni}^0(\text{P}^{\text{Cy}}_2\text{N}^{\text{Me}}_2\text{H})_2]^{2+}$ and $[\text{Ni}^0(\text{P}^{\text{tBu}}_2\text{N}^{\text{Me}}_2\text{H})_2]^{2+}$. A methyl substituent on the nitrogen was used instead of benzyl to reduce the computational cost.

Table 5. Oxidation Potentials for $[\text{Ni}(\text{P}^{\text{R}}_2\text{N}^{\text{R}'}_2\text{H})_2]^{2+}$ in MeCN

complex (R, R')	Ni(II/I)	exo-exo Ni(I/0) (V)	endo-exo Ni(I/0) (V)	endo-endo ^c Ni(I/0) (V)	Δ exo-exo vs endo-exo (mV)	Δ endo-exo vs endo-endo (mV)
Cy, Bn-OMe ^a	-0.85	-0.74	-0.33	-0.04	410	290
Cy, Bn-COOMe ^a	-0.69	-0.59	-0.24	0.01	350	250
Cy, Bn-Ala-OMe ^a	nd	-0.66	-0.27	-0.02	390	250
Cy, Bn-Phe-OMe ^a	nd	-0.65	-0.25	-0.02	400	230
^t Bu, Bn ^b		-0.61	-0.29	-0.12	320	170

^aOxidation peak potentials (E_p) of irreversible waves. ^b $E_{1/2}$ potentials of quasi-reversible waves previously determined by Wiedner et al.¹⁶ ^cPotential measured at half the maximum current of the wave.

These calculations indicate that there is increased hydrogen bonding stabilization in the $[\text{Ni}^0(\text{P}^{\text{Cy}}_2\text{N}^{\text{Me}}_2\text{H})_2]^{2+}$ complexes.

As can be inferred from Figure 8, because of the tetrahedral symmetry of the Ni⁰ complexes, the substituent on the

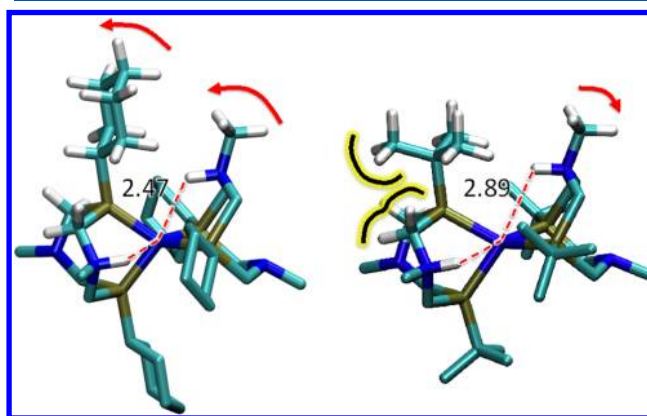


Figure 8. Optimized structure of the $[\text{Ni}^{\text{II}}(\text{P}^{\text{Cy}}_2\text{N}^{\text{Me}}_2\text{H})_2]^{2+}$ (left) and $[\text{Ni}^{\text{II}}(\text{P}^{\text{tBu}}_2\text{N}^{\text{Me}}_2\text{H})_2]^{2+}$ (right) endo-endo isomers. The red dotted lines show the $\text{NH}\cdots\text{Ni}$ hydrogen bond distance (in Å). The red arrows indicate the movement of the pendant amine and of the cyclohexyl group upon protonation. The steric interaction between the methyl group of the *tert*-butyl substituent and the CH_2 of the $\text{P}-\text{CH}_2-\text{N}$ linker is schematically indicated with black and yellow lines.

phosphorus atom of the ligand has to accommodate the protonated pendant amine of the other ligand, resulting in the phosphorus atom substituent moving away from the pendant amine upon protonation. In $[\text{Ni}^0(\text{P}^{\text{Cy}}_2\text{N}^{\text{Me}}_2\text{H})_2]^{2+}$ the smaller size of the cyclohexyl substituent allows the protonated amine to get closer to the metal center upon protonation, and the Ni–N distance decreases from 3.40 Å in the nonprotonated complex to 3.18 Å in the protonated complex. In contrast, the larger *tert*-butyl substituent is not able to accommodate the protonated pendant amine because of the steric clash between one of the methyl groups with the CH_2 groups of the $\text{P}-\text{CH}_2-\text{N}$ linker (Figure 8). Therefore, upon protonation to form $[\text{Ni}^0(\text{P}^{\text{tBu}}_2\text{N}^{\text{Me}}_2\text{H})_2]^{2+}$, the Ni–N distance slightly increases from 3.39 to 3.42 Å. As a result, the $\text{NH}\cdots\text{Ni}$ distances are reduced for the cyclohexyl-containing substituent (2.47 Å) in comparison to the *tert*-butyl substituent (2.89 Å). This is consistent with the experimentally observed increase in metal

hydrogen bonding stability of the endo-containing isomers of the $[\text{Ni}^{\text{II}}(\text{P}^{\text{Cy}}_2\text{N}^{\text{Bn-R}}_2\text{H})_2]^{2+}$ complexes. These results are also consistent with previous studies that have shown that increasing steric bulk on the ammonium moiety decreases the strength of metal hydrogen bonding in $\text{M}\cdots\text{H}-\text{N}$ bonds ($\text{M} = \text{Pt}(\text{II}), \text{Co}(-\text{I})$), as the ammonium moiety is pushed farther from the metal coordination sphere.^{26–29}

Catalytic Oxidation of H_2 by the $[\text{Ni}(\text{P}^{\text{Cy}}_2\text{N}^{\text{Bn-R}}_2)]$ Complexes. All complexes were observed to be catalytically active for H_2 oxidation, where the rate was measured both in benzonitrile and acetonitrile with added water, using triethylamine as the base (Figures 9 and 10, Figure S5 (Supporting

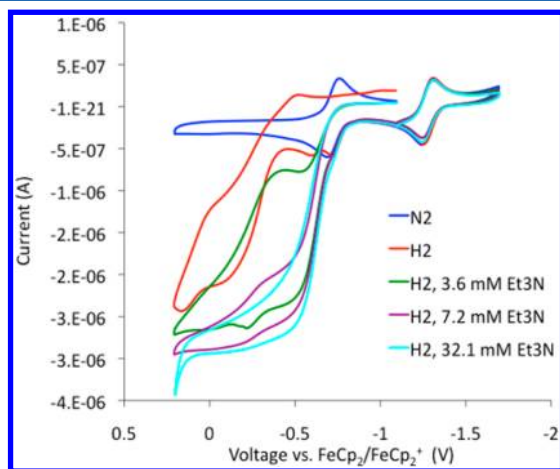


Figure 9. CV's for $[\text{Ni}(\text{P}^{\text{Cy}}_2\text{N}^{\text{Bn-OMe}}_2)]$ (0.75 mM) in PhCN with 0.2 M NBu_4PF_6 , showing catalytic activity at the Ni(II/I) couple upon the addition of H_2 and Et_3N . Data were taken at 50 mV s^{-1} and referenced vs $\text{FeCp}_2/\text{FeCp}_2^+$ using the potential of the Ni(I/0) couple.

Information)), and Table 4). In benzonitrile, the large increase in current at the potential assigned to the endo-endo isomer observed in the absence of base (red curve, Figure 9) is scan rate independent (Figure S6 (Supporting Information)) and is indicative of catalysis occurring at the I/0 oxidation of the endo-endo isomer of $[\text{Ni}(\text{P}^{\text{Cy}}_2\text{N}^{\text{Bn-R}}_2\text{H})_2]^{2+}$, as discussed in detail below. Upon the addition of triethylamine, the onset of catalysis shifts to more negative potentials (green, purple, and

turquoise curves, Figure 9), occurring slightly negative of the II/I couple, and is similar to previous studies of the parent complex in acetonitrile.¹⁰ In comparison to the parent complex, the rate decreases slightly with the methyl ester substituent and increases slightly with the methyl ether substituent (Table 4). This is the expected trend on the basis of the relative ΔG_{H_2} values if hydrogen addition is the rate-limiting step in catalysis.

In acetonitrile, the cyclic voltammograms for $[\text{Ni}(\text{P}^{\text{Cy}}_2\text{N}^{\text{Bn-OMe}}_2)]^{2+}$ displayed similar behavior, although in this solvent the rate of H_2 oxidation was slightly slower than for the parent complex, $[\text{Ni}(\text{P}^{\text{Cy}}_2\text{N}^{\text{Bn}}_2)]^{2+}$. Consistent with previous studies,¹⁷ the magnitude of the catalytic wave increases upon the addition of water, resulting in a 10–50% increase in rate (Table S2 (Supporting Information)), and the onset shifts to slightly more negative potentials.

In acetonitrile, $[\text{Ni}(\text{P}^{\text{Cy}}_2\text{N}^{\text{Bn-COOMe}}_2)]^{2+}$ exhibits a somewhat more complex catalytic wave (Figure S5 (Supporting Information)). In the presence of H_2 , the wave shows catalysis at the endo-endo isomer (offscale), as was observed in benzonitrile. Following addition of triethylamine under H_2 , the catalytic current continues to increase at the endo-endo and endo-exo isomer, but not at the Ni(II/I) couple as is seen for the other complexes.³⁰ Upon addition of water, the current increase at $\sim -0.3 \text{ V}$ (the endo-exo isomer) becomes larger, with the onset shifting to less positive potentials as more water is added, resulting in a rate of $\sim 2 \text{ s}^{-1}$ at the maximum current. This wave corresponds to a catalytic pathway different from that observed for the other complexes in the presence of H_2 , triethylamine, and water.

Hydrogen addition is calculated to be most favorable for $[\text{Ni}(\text{P}^{\text{Cy}}_2\text{N}^{\text{Bn-OMe}}_2)]^{2+}$ and least favorable for $[\text{Ni}(\text{P}^{\text{Cy}}_2\text{N}^{\text{Bn-COOMe}}_2)]^{2+}$ (Table 4). In this series of complexes, the rates of catalytic hydrogen oxidation measured in benzonitrile have the expected (slight) increase as ΔG_{H_2} becomes more favorable and, relatedly, the amine $\text{p}K_a$ of $[\text{Ni}^0(\text{P}^{\text{Cy}}_2\text{N}^{\text{Bn-R}}_2\text{H})_2]^{2+}$ increases. However, in acetonitrile, the methyl ether containing complex $[\text{Ni}(\text{P}^{\text{Cy}}_2\text{N}^{\text{Bn-OMe}}_2)]^{2+}$, expected to be fastest, is slower than $[\text{Ni}(\text{P}^{\text{Cy}}_2\text{N}^{\text{Bn}}_2)]^{2+}$. This result is unexpected if the addition of H_2 is the rate-limiting step and may suggest that there is another step in the catalytic cycle, such as deprotonation by the external base, that is controlling the rate.

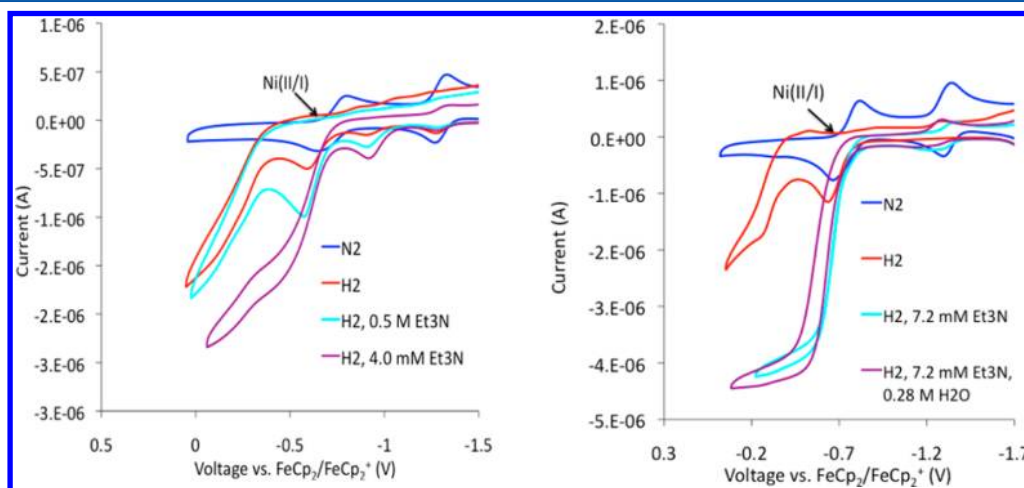


Figure 10. CV's for $[\text{Ni}(\text{P}^{\text{Cy}}_2\text{N}^{\text{Bn-Ala-OMe}}_2)]^{2+}$ in PhCN (left) and MeCN with added water (right) with 0.2 M NBu_4PF_6 . Data were taken at 50 mV/s and referenced vs Fc/Fc^+ using $[\text{CoCp}^*_2](\text{PF}_6)$; titrated with Et_3N ; [cat.] = 0.75 mM.

Upon addition of triethylamine to the amino acid ester containing complexes, the catalytic current increases in a manner similar to that for the other complexes, suggesting a similar mechanism (Figure 10). However, for the amino acid ester containing complexes, the catalytic wave continues to slope to increasingly negative currents rather than plateau (Figure 10, left). This is consistent with H₂ oxidation at the Ni(I/0) endo-endo and endo-exo isomers as well as at the Ni(II/I) couple. In acetonitrile, the addition of water results in a catalytic wave at the Ni(II/I) couple which plateaus (Figure 10, right). This is thought to be due to the ability of water to facilitate deprotonation of the endo-endo isomer to form the hydride.¹⁷ The reported catalytic rates were determined by measuring the i_{cat} value at the II/I couple.

$[\text{Ni}(\text{P}^{\text{Cy}}_2\text{N}^{\text{Bn-Ala-OMe}}_2)_2]^{2+}$ and $[\text{Ni}(\text{P}^{\text{Cy}}_2\text{N}^{\text{Bn-Phe-OMe}}_2)_2]^{2+}$ have ΔG_{H_2} values similar to that of $[\text{Ni}(\text{P}^{\text{Cy}}_2\text{N}^{\text{Bn-COOMe}}_2)_2]^{2+}$, and the complexes have comparable rates of hydrogen oxidation. While the ³¹P NMR spectroscopy results suggest that structural rearrangements may be hindered by the steric bulk of the amino acid ester complexes, these rates are still much faster than catalysis and are likely not contributing to rates that are slower than that for the parent complex. These results are expected if H₂ addition is the rate-limiting step and suggest that the observed modifications in rate are explained by a second coordination sphere effect ($\text{p}K_{\text{a}}$ of the pendant amine), rather than effects in the outer coordination sphere.

The outer coordination sphere in enzymes is thought to influence catalytic activity, due to both steric and electronic factors. For example, Happe et al. found that amino acids that interact with the dithiolate ligand in [FeFe]-hydrogenase strongly impact the structure and activity of the enzyme.³¹ Additionally, hydrogen bonding by outer coordination sphere serine and lysine residues to the active site CN⁻ ligands and steric effects from phenylalanine and other hydrophobic residues are hypothesized to prevent rearrangement of the [2Fe] subcluster during the catalytic cycle.^{32,33} For the $\text{Ni}(\text{P}^{\text{R}}_2\text{N}^{\text{R}}_2)_2$ catalysts, a steric influence that could enhance catalysis would be one which forced an endo conformation and limited boat–chair conformational isomerizations of the Ni–P–C–N–C–P chelate rings, a role which the protein scaffold may serve in hydrogenases. While the amino acid ester ligands here did slow boat to chair isomerizations, they were still orders of magnitude faster than catalysis. This is likely due to a lack of positioning of the appended amino acids, which undergo unrestricted conformational movements. A well-positioned and structurally less flexible outer coordination sphere such as that seen in enzymes is necessary to achieve the positioning which could result in the desired steric or electronic effects on the active site.

Role of Water As Base. For the Ni complexes containing methyl ester (Figure S5 (Supporting Information)), amino acid ester (Figure 10), and methyl ether groups (Figures 7 and 9), it was observed that under H₂ a scan-rate-independent (Figure S6 (Supporting Information)) current enhancement was observed at the Ni(0/I) oxidation for the endo-endo isomer, even in the absence of added base. The most likely source of an external base is residual water, and to test whether water could act as a base at this potential, CV's were collected as aliquots of water were added to $[\text{Ni}(\text{P}^{\text{Cy}}_2\text{N}^{\text{Bn-OMe}}_2)_2]^{2+}$ in acetonitrile under H₂ (Figure 11). As water was added, a scan-rate-independent current enhancement at the endo-endo isomer was observed,

confirming that water is able to act as a base to facilitate catalysis.

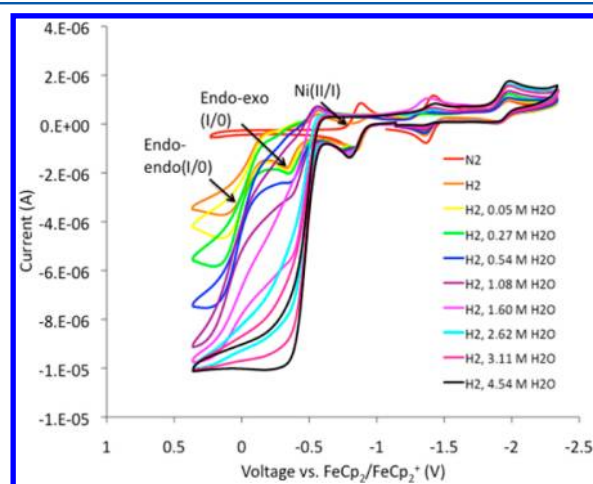


Figure 11. CV's for $[\text{Ni}(\text{P}^{\text{Cy}}_2\text{N}^{\text{Bn-OMe}}_2)_2]^{2+}$ in MeCN titrated with H₂O, showing that water is able to act as a base for the oxidation of H₂, albeit operating at a more positive potential. The wave at -1.94 V is due to $\text{CoCp}^*_{2/2+}$.

At low water concentrations, the current enhancement was located at the potential of the endo-endo isomer. At intermediate water concentrations, a current enhancement could also be seen at the oxidation potential of the endo-exo isomer of $[\text{Ni}(\text{P}^{\text{Cy}}_2\text{N}^{\text{Bn-OMe}}_2)_2]^{2+}$ (Figure 11). At the highest concentrations of water (4.5 M) the current enhancement occurs only near the endo-exo oxidation potential, giving a maximum $i_{\text{c}}/i_{\text{p}}$ ratio of 8.5. This shift in potential can be explained if isomerization from the endo-endo isomer to the endo-exo isomer occurs faster than catalysis at these concentrations of water, resulting in the oxidation and subsequent deprotonation by water of the endo-exo isomer. The maximum rate for H₂ oxidation using water as a base was 8.8 s^{-1} , similar to the rate when triethylamine is used as a base. Upon addition of triethylamine to this solution, the catalytic wave shifts cathodically to the Ni(II/I) couple, as expected in the presence of a strong base (Figure S7 (Supporting Information)).

Water is unlikely to act as a base for $[\text{Ni}(\text{P}^{\text{Cy}}_2\text{N}^{\text{Bn-OMe}}_2)_2]^{2+}$ because of its low $\text{p}K_{\text{a}}$ value. Therefore, in contrast to the situation where a strong base is used (Figure 9), oxidation of $[\text{Ni}(\text{P}^{\text{Cy}}_2\text{N}^{\text{Bn-OMe}}_2)_2]^{2+}$ must occur before proton transfer. The pendant amine of the resulting oxidized product, $[\text{Ni}(\text{P}^{\text{Cy}}_2\text{N}^{\text{Bn-OMe}}_2)_2]^{3+}$, is expected to have a lower $\text{p}K_{\text{a}}$,¹⁴ allowing water to remove a proton. Therefore, the sequence of events when water acts as a base is altered from the sequence shown in Scheme 1 and could be (1) $\text{e}^- \text{H}^+ \text{e}^- \text{H}^+$, (2) $\text{e}^- \text{H}^+ \text{H}^+ \text{e}^-$, or (3) $\text{e}^- \text{e}^- \text{H}^+ \text{H}^+$.

Similar current enhancements were seen upon titration of $[\text{Ni}(\text{P}^{\text{Cy}}_2\text{N}^{\text{Bn}}_2)_2]^{2+}$ and $[\text{Ni}(\text{P}^{\text{Cy}}_2\text{N}^{\text{Bn-COOMe}}_2)_2]^{2+}$ with water under H₂ (2.9 and 1.7 s^{-1} , respectively), suggesting that using water as a base for catalysis should be generalizable to this class of hydrogen oxidation catalysts. However, the fastest rates were observed with $[\text{Ni}(\text{P}^{\text{Cy}}_2\text{N}^{\text{Bn-OMe}}_2)_2]^{2+}$. It is possible that the methoxy group contained by the ligand assists in deprotonation of the pendant amine by water. These results are extremely encouraging for the development of molecular first row transition metal containing H₂ oxidation catalysts that use

water, an economical and environmentally friendly reagent, as a base.

CONCLUSIONS

In the derivatives studied here, rate enhancements were not observed for catalysts derivatized with amino acid esters. Although conformational flexibility was reduced for these catalysts, rates for these processes were orders of magnitude faster than catalysis and the slight variations in rate observed could be explained by electronic effects in the second coordination sphere. Several mechanistic observations will be important to consider for future catalyst design. For example, the sequence of catalytic events can be altered by using a weak base, deprotonation may be the rate-limiting step in some cases, and isomerization could control the potential at which the catalyst operates.

$\text{Ni}(\text{P}^{\text{R}}_2\text{N}^{\text{R}'}_2)_2$ hydrogen production catalysts containing amino acids or amino acid esters in the outer coordination sphere showed rates several times faster than that of the parent catalyst.¹⁸ This may be due to the ability of these groups to create a localized increase in proton concentration around the catalyst due to their protic nature or to their ability to increase water concentration around the catalyst.³⁴ A localized increase in protons would not be expected to facilitate hydrogen oxidation, but rates can potentially be increased by adding Brønsted bases in the outer coordination sphere to facilitate the shuttling of protons from the active site to an external base. As deprotonation becomes rate limiting, observed in one catalyst reported here, a proton channel will be an essential feature to enhance catalytic rates. The complexes developed here provide the foundation to attach such a coordination sphere.

EXPERIMENTAL SECTION

General Procedures. Solution-state ^1H and ^{31}P NMR spectra were recorded on Varian VNMR spectrometers (500 or 300 MHz ^1H frequency). All ^1H chemical shifts were internally calibrated to the monoprotic solvent impurity. Elemental analyses were performed by Atlantic Microlab, Norcross, GA, with V_2O_5 as a combustion catalyst. Electrospray ionization (ESI) and atomic pressure chemical ionization (APCI) were collected at the Indiana University Mass Spectrometry Facility on a Waters/Micromass LCT Classic using anhydrous solvents and inert-atmosphere techniques.

Synthesis and Materials. All reactions were performed using standard Schlenk techniques or in a glovebox under a N_2 atmosphere. Deoxygenated acetonitrile, diethyl ether, and THF were dried using an Innovative Technology, Inc. PureSolv solvent purification system. Ethanol, methanol, water, and triethylamine used in syntheses were not dried but were degassed by sparging with N_2 overnight prior to use. *O*-(Benzotriazol-1-yl)-*N,N,N',N'*-tetramethyluronium tetrafluoroborate (TBTU), *L*-alanine methyl ester hydrochloride (H-Ala-OMe-HCl), and *L*-phenylalanine methyl ester hydrochloride (H-Phe-OMe-HCl) were purchased from EMD Chemicals, Inc. Methyl 4-(aminomethyl)benzoate hydrochloride, benzylamine, and *p*-methoxybenzylamine were purchased from SigmaAldrich. Liquid reagents were deoxygenated by sparging with N_2 for several hours, and solid reagents were placed under alternating cycles of vacuum and N_2 before use. $\text{CyP}(\text{CH}_2\text{OH})_2$ was synthesized according to a literature procedure,²¹ as was $[\text{Ni}(\text{CH}_3\text{CN})_6](\text{BF}_4)_2$.³⁵

$\text{P}^{\text{Cy}}_2\text{N}^{\text{Bn-COOMe}}_2$. Methyl 4-(aminomethyl)benzoate hydrochloride (143.2 mg, 0.71 mmol) and triethylamine (0.11 mL, 0.78 mmol) were combined in a Schlenk flask with 5 mL of ethanol and heated to 65 °C until the reagents had dissolved. $\text{CyP}(\text{CH}_2\text{OH})_2$ (125.0 mg, 0.71 mmol) dissolved in 3 mL of ethanol was then added dropwise over 25 min. The reaction mixture was further heated at 65 °C for 22 h, during which time the product appeared as a white precipitate. The reaction

was then cooled to room temperature and brought into a glovebox under a nitrogen atmosphere. The white precipitate was collected on a fritted funnel by vacuum filtration, washed with 3 mL of additional ethanol, and then dried under vacuum. Yield: 170.4 mg, 79%. $^{31}\text{P}\{^1\text{H}\}$ NMR (CD_2Cl_2): δ -60 ppm, broad. ^1H NMR (CD_2Cl_2): δ (ppm) 7.96 (4H, d, J = 8 Hz, Ar-H), 7.44 (4H, d, J = 8 Hz, Ar-H), 3.96 (4H, s, NCH_2Ph), 3.88 (6H, s, CO_2CH_3), 3.13 (8H, s, PCH_2N), 0.9–1.7 (22 H, m, Cy-H). APCI MS: m/z ($\text{P}^{\text{Cy}}_2\text{N}^{\text{Bn-COOMe}}_2 + \text{H}^+$) 611.319 (calcd 611.317).

$\text{P}^{\text{Cy}}_2\text{N}^{\text{Bn-COO-Li}}_2$. $\text{P}^{\text{Cy}}_2\text{N}^{\text{Bn-COOMe}}_2$ (250 mg, 0.4 mmol) was dissolved in 16.9 mL of THF in a Schlenk flask. MeOH (8.4 mL) and 1 M aqueous LiOH (2.4 mL) were added, and the reaction mixture was heated to 50 °C for 5 h. The reaction mixture was then cooled and transferred to a glovebox. The white precipitate product was collected on a fritted funnel by vacuum filtration, washed with additional THF (~5 mL), and then dried under vacuum. Yield: 154.9 mg, 65%. $^{31}\text{P}\{^1\text{H}\}$ NMR (D_2O): δ -68 ppm. ^1H NMR (D_2O): δ (ppm) 7.83 (4H, d, J = 8 Hz, Ar-H), 7.35 (4H, d, J = 8 Hz, Ar-H), 3.98 (4H, s, NCH_2Ph), 3.17 (4H, d, J = 14.5 Hz, PCH_2N), 3.06 (4H, d, J = 14.5 Hz, PCH_2N), 1.54–0.82 (22H, m, Cy-H). ESI MS: m/z ($\text{P}^{\text{Cy}}_2\text{N}^{\text{Bn-COO-Li}}_2 - 2 \text{Li}^+ + \text{H}^+$) 581.270 (calcd 581.271).

$[\text{Ni}(\text{P}^{\text{Cy}}_2\text{N}^{\text{Bn-COOMe}}_2)_2](\text{BF}_4)_2$. $\text{P}^{\text{Cy}}_2\text{N}^{\text{Bn-COOMe}}_2$ (100 mg, 0.164 mmol) and $[\text{Ni}(\text{CH}_3\text{CN})_6](\text{BF}_4)_2$ (39.2 mg, 0.082 mmol) were combined in ~3 mL of MeCN and stirred overnight. Recrystallization by slow diffusion of ether into the MeCN solution gave dark reddish purple blocklike crystals in quantitative yield. $^{31}\text{P}\{^1\text{H}\}$ NMR (CH_3CN): δ 10 ppm. ^1H NMR (D_2O): δ (ppm) 8.01 (8H, d, J = 8 Hz, Ar-H), 7.31 (8H, d, J = 8 Hz, Ar-H), 3.88 (12H, s, CO_2CH_3), 3.66 (4H, d, J = 13 Hz, NCH_2Ph), 3.43 (4H, d, J = 13 Hz, NCH_2Ph), 3.10 (4H, d, J = 13 Hz, PCH_2N), 2.90 (4H, d, J = 12 Hz, PCH_2N), 2.79 (4H, d, J = 13 Hz, PCH_2N), 2.61 (4H, d, J = 11 Hz, PCH_2N), 2.14–1.05 (m, 44H, Cy-H). Anal. Calcd for $\text{C}_{68}\text{H}_{96}\text{B}_2\text{F}_8\text{N}_4\text{NiO}_8\text{P}_4$: C, 56.18; H, 6.66; N, 3.85. Found: C, 56.10; H, 6.87; N, 3.88. ESI MS: m/z $\{[\text{Ni}(\text{P}^{\text{Cy}}_2\text{N}^{\text{Bn-COOMe}}_2)_2](\text{BF}_4)_2\}^+$ 1365.554 (calcd 1365.556).

$\text{Ni}(\text{P}^{\text{Cy}}_2\text{N}^{\text{Bn-COOMe}}_2)_2$. Tetramethylguanidine (19.8 mg, 0.1722 mmol) was added to $[\text{Ni}(\text{P}^{\text{Cy}}_2\text{N}^{\text{Bn-COOMe}}_2)_2](\text{BF}_4)_2$ (119.2 mg, 0.082 mmol) in ~3 mL of MeCN. H_2 was then bubbled through the solution for 10 min. The reaction mixture was allowed to sit for several days, during which time $\text{Ni}(\text{P}^{\text{Cy}}_2\text{N}^{\text{Bn-COOMe}}_2)_2$ precipitated as a yellow solid (58 mg, 49% yield). When the reaction was run on a smaller scale (0.0318 mmol of $[\text{Ni}(\text{P}^{\text{Cy}}_2\text{N}^{\text{Bn-COOMe}}_2)_2]^{2+}$), $\text{Ni}(\text{P}^{\text{Cy}}_2\text{N}^{\text{Bn-COOMe}}_2)_2$ precipitated as X-ray-quality yellow-orange crystals. $^{31}\text{P}\{^1\text{H}\}$ NMR (CH_2Cl_2): δ 11.1 ppm. ^1H NMR (THF- d_6): δ (ppm) 7.93 (8H, d, J = 6.5 Hz, Ar-H), 7.16 (8H, d, J = 7.5 Hz, Ar-H), 3.91 (12H, s, CO_2CH_3), 3.71 (8H, s, NCH_2Ph), 2.67 (8H, d, J = 10.5 Hz, PCH_2N), 2.41 (8H, d, J = 11.5 Hz, PCH_2N), 1.77–1.14 (44H, m, Cy-H). Anal. Calcd for $\text{C}_{68}\text{H}_{96}\text{N}_4\text{NiO}_8\text{P}_4$: C, 63.80; H, 7.56; N, 4.38. Found: C, 63.78; H, 7.60; N, 4.43.

$\text{P}^{\text{Cy}}_2\text{N}^{\text{Bn-Ala-OMe}}_2$. $\text{P}^{\text{Cy}}_2\text{N}^{\text{Bn-COO-Li}}_2$ (50 mg, 0.084 mmol) and TBTU (59.4 mg, 0.185 mmol) were stirred together for 15 min in ~2.5 mL of CH_2Cl_2 . H-Ala-OMe-HCl (24.7 mg, 0.176 mmol) and triethylamine (0.03 mL) were combined in a separate flask in ~5 mL of CH_2Cl_2 , and then added to the $\text{P}^{\text{Cy}}_2\text{N}^{\text{Bn-COO-Li}}_2$ and TBTU in a dropwise manner. The mixture was stirred for an additional 20 h, followed by collection of the white precipitate on a fritted glass funnel. The product was washed with water (10 mL) and dichloromethane (10 mL) and dried under vacuum. Yield: 54.5 mg, 86%. $^{31}\text{P}\{^1\text{H}\}$ NMR (THF): δ -60.3 ppm. ^1H NMR (THF- d_6): δ (ppm) 7.81 (4H, d, J = 7.5 Hz, Ar-H), 7.74 (2H, d, J = 7.5 Hz, amide-H), 7.41 (4H, d, J = 7.5 Hz, Ar-H), 4.70 (2H, m, $\text{C}_\alpha\text{-H}$), 4.00 (4H, s, NCH_2Ph), 3.67 (6H, s, CO_2CH_3), 3.19 (8H, s, PCH_2N), 1.60 (6H, s, J = 7.2 Hz, $\text{C}_\alpha\text{-CH}_3$), 1.87–1.00 (22H, m, Cy-H). APCI MS: m/z ($\text{P}^{\text{Cy}}_2\text{N}^{\text{Bn-Ala-OMe}}_2 + \text{H}^+$) 753.391 (calcd 753.391).

$[\text{Ni}(\text{P}^{\text{Cy}}_2\text{N}^{\text{Bn-Ala-OMe}}_2)_2](\text{BF}_4)_2$. $\text{P}^{\text{Cy}}_2\text{N}^{\text{Bn-Ala-OMe}}_2$ (55.5 mg, 0.074 mmol) and $[\text{Ni}(\text{CH}_3\text{CN})_6](\text{BF}_4)_2$ (17.6 mg, 0.037 mmol) were combined in 2 mL of MeCN and stirred for 3 days. The deep purple mixture was then filtered, and the material in the filtrate precipitated by addition of diethyl ether (~20 mL). The purple solid was collected on a frit, washed with additional diethyl ether (~10 mL), and then dried under vacuum for several hours. Yield: 40 mg, 72%. $^{31}\text{P}\{^1\text{H}\}$

NMR (CD₃CN): δ 0 ppm (broad). ¹H NMR (CD₃CN): δ (ppm) 7.86 (8H, d, J = 8 Hz, Ar-H), 7.68 (4H, d, J = 6.5 Hz, amide-H), 7.23 (8H, d, J = 7.5 Hz, Ar-H), 4.60 (4H, m, C_α-H), 3.73 (12H, s, CO₂CH₃), 3.68 (8H, d, J = 7 Hz, NCH₂Ph), 3.02 (4H, d, J = 13 Hz, PCH₂N), 2.91 (4H, d, J = 12.5 Hz, PCH₂N), 2.81 (4H, dd, J = 4.5 Hz, 13 Hz, PCH₂N), 2.65 (4H, d, J = 11.5 Hz, PCH₂N), 1.52 (12H, m, C_αCH₃), 2.02–1.11 (44 H, m, Cy-H). ESI MS: m/z {[Ni(P^{Cy}₂N^{Bn-Ala-OMe}₂)](BF₄)⁺} 1649.700 (calcd 1649.706).

P^{Cy}₂N^{Bn-Phe-OMe}₂, P^{Cy}₂N^{Bn-COO-Li}₂ (50 mg, 0.084 mmol) and TBTU (59.4 mg, 0.185 mmol) were stirred together for 15 min in ~4 mL of CH₂Cl₂. H-Phe-OMe-HCl (90.6 mg, 0.42 mmol) and triethylamine (0.07 mL) in ~3 mL of CH₂Cl₂ were then added. The reaction mixture was stirred for an additional 18 h at room temperature and was then filtered. The solvent was removed under vacuum, and the resulting residue was washed with H₂O and MeCN (20 mL each) and then dried under vacuum, giving a yield of 19.3 mg (25% yield). ³¹P{¹H} NMR (CD₂Cl₂): δ 59 ppm (broad). ¹H NMR (CD₂Cl₂): δ (ppm) 7.66 (4H, d, J = 8.4 Hz, Ar-H), 7.42 (4H, d, J = 8.4 Hz, Ar-H), 7.28 (6H, m, phenylalanine-H), 7.16 (4H, m, phenylalanine-H), 6.55 (2H, d, J = 7.5 Hz, amide-H), 5.02 (2H, ddd, J = 11.55 Hz, 6 Hz, 1.8 Hz, C_α-H), 3.94 (4H, s, NCH₂Ph), 3.75 (6H, s, CO₂CH₃), 3.28 (2H, dd, J = 8.1 Hz, 5.7 Hz, C_αCH₂Ph), 3.19 (2H, dd, J = 8.1 Hz, 5.7 Hz, C_αCH₂Ph), 3.12 (8H, s, PCH₂N), 0.90–1.65 (22 H, m, Cy-H).

[Ni(P^{Cy}₂N^{Bn-Phe-OMe}₂)](BF₄)₂, P^{Cy}₂N^{Bn-Phe-OMe}₂ (19.3 mg, 0.021 mmol) and [Ni(CH₃CN)₆](BF₄)₂ (5.1 mg, 0.011 mmol) were combined in ~1 mL of acetonitrile. The reaction mixture was stirred for 3 days and then filtered. The product was obtained by removal of the solvent from the filtrate under vacuum. Yield: 0.0216 g, 99%. ³¹P{¹H} NMR (CD₃CN): δ 10 ppm (very broad). ¹H NMR (CD₃CN): δ (ppm) 7.71 (8H, d, J = 7.5 Hz, Ar-H), 7.64 (4H, m, amide-H), 7.15–7.26 (28H, m, Ar-H), 4.87 (4H, m, C_α-H), 3.68 (8H, m, NCH₂Ph), 3.64 (12H, s, CO₂CH₃), 3.19 (8H, m, C_αCH₂Ph), 2.98–2.59 (16H, m, PCH₂N), 2.10–0.88 (44H, Cy-H). ESI MS: m/z [Ni(P^{Cy}₂N^{Bn-Phe-OMe}₂)]²⁺ 933.896 (calcd 933.915).

Ni(P^{Cy}₂N^{Bn-OMe}₂)₂, CyP(CH₂OH)₂ (125.0 mg, 0.71 mmol) in 6 mL of ethanol was added dropwise to 4-methoxybenzylamine in 6 mL of ethanol at 65 °C. The reaction mixture was stirred at 65 °C overnight. The reaction mixture was then cooled to room temperature, and the ethanol was removed under vacuum. The crude ligand was combined with [Ni(CH₃CN)₆](BF₄)₂ (84.9 mg, 0.1775 mmol) in ~5 mL of acetonitrile and stirred for 1 week. The reaction mixture was filtered, and tetramethylguanidine (45.0 mg, 0.3905 mmol) was added to the filtrate. Hydrogen was bubbled through the filtrate, and the reaction mixture was allowed to sit for 4 days, during which time Ni(P^{Cy}₂N^{Bn-OMe}₂)₂ precipitated as a yellow solid. The product was washed with additional acetonitrile (~20 mL) and dried under vacuum. Yield: 65.1 mg, 31.4%. ³¹P{¹H} NMR (THF): δ (ppm) 10.1. ¹H NMR (THF-*d*₆): δ (ppm) 6.97 (8H, d, J = 8.5 Hz, Ar-H), 6.80 (8H, d, J = 8.5 Hz, Ar-H), 3.79 (s, 12H, OCH₃), 3.58 (s, 8H, NCH₂Ph), 2.68 (8H, d, J = 9.5 Hz, PCH₂N), 2.34 (8H, d, J = 11 Hz, PCH₂N), 1.77–1.11 (m, 44H, Cy-H). Anal. Calcd for C₆₄H₉₆N₄NiO₄P₄: C, 65.81; H, 8.28; N, 4.80. Found: C, 65.78; H, 8.25; N, 4.75.

[Ni(P^{Cy}₂N^{Bn-OMe}₂)](BF₄)₂, [Ni(P^{Cy}₂N^{Bn-OMe}₂)]₂ (51.0 mg, 0.044 mmol) and ferrocenium tetrafluoroborate (FcCp₂⁺BF₄⁻) (24.1 mg, 0.088 mmol) were weighed into separate vials. Acetonitrile (1 mL) was added to each vial, and the FcBF₄ solution was then added to the Ni(P^{Cy}₂N^{Bn-OMe}₂)₂ suspension, and 1 mL of additional acetonitrile was used for transfer. The reaction mixture was stirred overnight, during which time the majority of the solid dissolved. The solution was then concentrated until ferrocene began precipitating as an orange solid. The reaction mixture was stored at –35 °C overnight. The mother liquor was removed by pipet, concentrated to dryness, and slurried with diethyl ether overnight. The ether was decanted and the solid dissolved in acetonitrile, followed by recrystallization by slow diffusion of ether into the solution. The product crystallized as red-purple needlelike crystals (30.0 mg, 51.2% yield). Recrystallization by slow diffusion of ether into an acetonitrile solution of the product on a smaller scale yielded X-ray-quality crystals. ³¹P{¹H} NMR (CD₃CN): δ (ppm) 9.2 (broad). ¹H NMR (CD₃CN): δ (ppm) 7.11 (8H, d, J

8.7 Hz, Ar-H), 6.93 (8H, d, J = 8.7 Hz, Ar-H), 3.79 (12H, s, OCH₃), 3.61 (4H, d, J = 12.9 Hz, NCH₂Ph), 3.45 (4H, d, J = 12.6 Hz, NCH₂Ph), 3.09 (4H, d, J = 13.8 Hz, PCH₂N), 2.88 (4H, d, J = 12.6 Hz, PCH₂N), 2.69 (4H, d, J = 13.5 Hz, PCH₂N), 2.55 (4H, d, J = 12.5 Hz, PCH₂N), 1.97–0.99 (44H, m, Cy-H). Anal. Calcd for C₆₇H_{100.5}B₂F₈N_{5.5}NiO₄P₄ ([Ni(P^{Cy}₂N^{Bn-OMe}₂)](BF₄)₂ + 1.5SCH₃CN): C, 57.35; H, 7.22; N, 5.49. Found: C, 57.22; H, 7.44; N, 5.46.

pK_a Measurements. The pK_a values for the pendant amine of [Ni(P^{Cy}₂N^{R'}₂H)₂]⁺, where R' = Bn-COOE, Bn-OMe, were determined by first vortexing [Ni(P^{Cy}₂N^{Bn-R'}₂)]₂ and 1.1 equiv of *p*-anisidinium tetrafluoroborate in CD₃CN to form the nickel hydride, with a concentration <10 mM. This solution was then titrated with a solution of *p*-anisidinium tetrafluoroborate in CD₃CN, and the ¹H and ³¹P NMR spectra were recorded after the addition of each aliquot (~0.1 equiv). The pK_a was calculated using eq 1

$$pK_a = pK_a(\text{anisidine}) - \log\left(\frac{[\text{HB}^+][\text{A}^-]}{[\text{B}][\text{HA}]}\right) \quad (1)$$

where A⁻ = [HNi(P^{Cy}₂N^{Bn-R}₂)]⁺, HA = [Ni(P^{Cy}₂N^{Bn-R}₂H)₂]²⁺, HB⁺ = *p*-anisidinium, B = anisidine, and [HB⁺]/[B] = (δ_{obs} – δ_B)/(δ_{HB⁺} – δ_{obs}).

The pK_a of the pendant amine for [Ni(P^{Cy}₂N^{Bn-R}₂H)₂]²⁺, where R = –COOMe, –Ala-OMe, –Phe-OMe, were calculated in the reverse direction: [Ni(P^{Cy}₂N^{Bn-R}₂)]²⁺ was dissolved in CD₃CN. The solution was sparged with H₂ to form [Ni(P^{Cy}₂N^{Bn-R}₂H)₂]²⁺ and then titrated with *p*-anisidine to form [HNi(P^{Cy}₂N^{Bn-R}₂)]⁺. The pK_a was then calculated using the above equations. In the case of [Ni(P^{Cy}₂N^{Bn-Ala-OMe}₂)]²⁺ and [Ni(P^{Cy}₂N^{Bn-Phe-OMe}₂)]²⁺, the nickel hydride appeared upon addition of H₂, before addition of the base, likely due either to residual H₂O from the synthesis or the ligand itself acting as a base. This results in an underestimation of the pK_a value, with an estimated error of ±0.5 pK_a units. Attempts to thoroughly dry these two complexes by recrystallizing, washing with diethyl ether, and placing the complexes under vacuum did not reduce the amount of hydride observed initially.

The pK_a for the metal hydride of [HNi(P^{Cy}₂N^{Bn-OMe}₂)]⁺ was measured by titration of a benzonitrile solution of [Ni(P^{Cy}₂N^{Bn-OMe}₂)]₂ with *N,N,N',N'*-tetramethylguanidinium tetrafluoroborate (HTMG·BF₄), where the ¹H and ³¹P NMR spectra of the solution were recorded after the addition of each aliquot (~0.1 equiv). Benzonitrile was used, since [Ni(P^{Cy}₂N^{Bn-OMe}₂)]₂ is not soluble in acetonitrile. The pK_a was calculated in a fashion analogous to that used for the pendant amine. Specifically, using eq 2

$$pK_a = pK_a(\text{TMG}) - \log\left(\frac{[\text{HB}^+][\text{A}^-]}{[\text{B}][\text{HA}]}\right) \quad (2)$$

where A⁻ = Ni(P^{Cy}₂N^{Bn-OMe}₂), HA = [HNi(P^{Cy}₂N^{Bn-OMe}₂)]⁺, HB⁺ = HTMG⁺, B = TMG, and [HB⁺]/[B] = (δ_{obs} – δ_B)/(δ_{HTMG⁺} – δ_{obs}).

Electrochemical Studies. All cyclic voltammetry experiments were carried out on a computer-aided CH Instruments 1100 A potentiostat in a glovebox with an N₂ atmosphere in 0.2 M ⁿBu₄N⁺PF₆⁻/acetonitrile or benzonitrile solutions at a scan rate of 50 mV/s, unless otherwise noted. The working electrode used was a glassy-carbon disk, and the counter electrode was a glassy-carbon rod. A silver wire was used as a pseudo reference electrode.

Decamethylcobaltocenium hexafluorophosphate (CoCp*₂⁺PF₆⁻, –1.94 V vs FeCp₂⁺⁰ in acetonitrile) or cobaltocenium hexafluorophosphate (CoCp₂⁺PF₆⁻, –1.33 vs FeCp₂⁺⁰ in acetonitrile) were used as internal standards to reference the potentials of the Ni(II/I) and Ni(I/0) redox couples to the ferrocenium/ferrocene couple. The benzonitrile used for electrochemical measurements was purchased from SigmaAldrich and filtered through activated alumina before use. The triethylamine used for electrochemical measurements was distilled over CaH₂ and then degassed using the freeze–pump–thaw method. Three trials were run for each type of catalyst in both benzonitrile and acetonitrile, and the rates from each trial were averaged. At least one trial in each set was run with either CoCp₂⁺ or CoCp*₂⁺ as an internal reference, and at least one trial in each set was run without addition of an internal reference in order to ensure that the internal reference did not influence the rates measured. [Ni^I(P^{Cy}₂N^{Bn-OMe}₂)](BF₄) for

electrochemical measurements was synthesized by stirring 1 equiv each of $[\text{Ni}^0(\text{P}^{\text{Cy}}_2\text{N}^{\text{Bn-OMe}}_2)_2]$ and $[\text{Ni}^{\text{II}}(\text{P}^{\text{Cy}}_2\text{N}^{\text{Bn-OMe}}_2)_2](\text{BF}_4)_2$ in the electrolyte-containing acetonitrile solution immediately before measurement.

Calculations. For the majority of the $[\text{HNi}(\text{P}^{\text{Cy}}_2\text{N}^{\text{Bn-R}}_2)_2]^+$ complexes, the hydride $\text{p}K_{\text{a}}$ values ($\text{p}K_{\text{a}}(\text{NiH})$) were calculated using a correlation between the $\text{p}K_{\text{a}}(\text{NiH})$ and the $E_{1/2}^{1/0}$ derived from several similar $[\text{HNi}(\text{P}^{\text{R}}_2\text{N}^{\text{R}'_2})_2]^+$ complexes:³⁶

$$\text{p}K_{\text{a}}(\text{Ni-H}) = -18.6 \times E_{1/2}^{1/0} - 2.65 \quad (3)$$

ΔG_{H^-} was calculated using a correlation between ΔG_{H^-} and $E_{1/2}^{\text{II/I}}$:³⁶

$$\Delta G_{\text{H}^-} (\text{kcal/mol}) = 20.8 \times E_{1/2}^{\text{II/I}} + 76.8 \quad (4)$$

ΔG_{H_2} was calculated using the thermodynamic cycle for H_2 addition described previously:¹⁰

$$\Delta G_{\text{H}_2} (\text{kcal/mol}) = \Delta G_{\text{H}^-} + 1.364 \\ \text{p}K_{\text{a}}([\text{Ni}^0(\text{P}^{\text{Cy}}_2\text{N}^{\text{Bn-R}}_2\text{H})_2]^{2+}) - 76 \quad (5)$$

In the case of $[\text{HNi}(\text{P}^{\text{Cy}}_2\text{N}^{\text{Bn-OMe}}_2)_2]^+$, the $\text{p}K_{\text{a}}$ was also experimentally measured (described above). Using the measured $\text{p}K_{\text{a}}$, $\Delta G(\text{H}^-)$ was calculated using the thermodynamic cycle described in Table 6.

Table 6. Calculation of $\Delta G(\text{H}^-)$

step	ΔG_{H^-} (kcal/mol)
$[\text{HNi}^{\text{II}}(\text{P}^{\text{Cy}}_2\text{N}^{\text{Bn-OMe}}_2)_2]^+ \rightarrow [\text{Ni}^0(\text{P}^{\text{Cy}}_2\text{N}^{\text{Bn-OMe}}_2)_2] + \text{H}^+$	$1.364 \times \text{p}K_{\text{a}}(\text{NiH})^{37}$
$[\text{Ni}^0(\text{P}^{\text{Cy}}_2\text{N}^{\text{Bn-OMe}}_2)_2] \rightarrow [\text{Ni}^{\text{I}}(\text{P}^{\text{Cy}}_2\text{N}^{\text{Bn-OMe}}_2)_2]^+ + \text{e}^-$	$23.06 \times E^{1/0}_{1/2}{}^{37}$
$[\text{Ni}^{\text{I}}(\text{P}^{\text{Cy}}_2\text{N}^{\text{Bn-OMe}}_2)_2]^+ \rightarrow [\text{Ni}^{\text{II}}(\text{P}^{\text{Cy}}_2\text{N}^{\text{Bn-OMe}}_2)_2]^{2+} + \text{e}^-$	$23.06 \times E^{\text{II/I}}_{1/2}{}^{37}$
$\text{H}^+ + 2\text{e}^- \rightarrow \text{H}^-$	79.6^{38}
$[\text{HNi}^{\text{II}}(\text{P}^{\text{Cy}}_2\text{N}^{\text{Bn-OMe}}_2)_2]^+ \rightarrow [\text{Ni}^{\text{II}}(\text{P}^{\text{Cy}}_2\text{N}^{\text{Bn-OMe}}_2)_2] + \text{H}^-$	

X-ray Crystallography. Crystals were mounted on a MiTeGen MicroMounts pin using Paratone-N oil and cooled to the data collection temperature (173 K for $[\text{Ni}(\text{P}^{\text{Cy}}_2\text{N}^{\text{Bn-COOMe}}_2)_2]$, $[\text{Ni}(\text{P}^{\text{Cy}}_2\text{N}^{\text{Bn-OMe}}_2)_2]$, and $[\text{Ni}(\text{P}^{\text{Cy}}_2\text{N}^{\text{Bn}}_2)_2]$; 120 K for $[\text{Ni}(\text{P}^{\text{Cy}}_2\text{N}^{\text{Bn-OMe}}_2)_2](\text{BF}_4)_2$ and $[\text{Ni}(\text{P}^{\text{Cy}}_2\text{N}^{\text{Bn-OMe}}_2)_2](\text{BF}_4)_2$). Data were collected on a Bruker-AXS II CCD diffractometer with 0.710 73 Å Mo $\text{K}\alpha$ radiation. Cell parameters were retrieved using Bruker APEX II software,³⁹ raw data were integrated using SAINTPlus,⁴⁰ and absorption correction was applied using SADABS.⁴¹ The structures were solved using either direct methods or the Patterson method and refined by a least-squares method on F^2 using the SHELXTL program package. Space groups were chosen by analysis of systematic absences and intensity statistics.⁴²

NMR Peak Fitting. The data was analyzed using the procedure described by O'Hagan et al.,²³ using gNMR for variable-temperature ^{31}P line shape analysis using a two-site exchange model.⁴³ Experimental spectra were processed within gNMR using a Lorentzian function with 4 Hz line broadening. Rates were determined by iteration of the simulated line widths, using both manual and gNMR algorithm methods. Visual inspection of the overlaid experimental and simulated spectra were used to determine the best fit.

The data were fit with the nonlinearized Eyring equation using Profit, which allowed the application of individual error bars determined for each data point in calculating error. Error bars for individual data points were estimated to be 10–15% on the basis of visual inspection of the gNMR fits.⁴⁴ Rate constants at the coalescence temperatures T_c were calculated using the equation $k_c = \pi\Delta\nu/\sqrt{2}$, where k_c is the rate constant at the coalescence temperature and $\Delta\nu$ is the line separation in the low-temperature limit.⁴⁵

Ab Initio Calculations. Ab initio calculations were performed in a manner similar to those previously reported.¹⁶ The structures of the $[\text{Ni}^0(\text{P}^{\text{Cy}}_2\text{N}^{\text{Me}}_2\text{H})_2]^{2+}$ endo-endo isomer and of $[\text{Ni}^0(\text{P}^{\text{Cy}}_2\text{N}^{\text{Me}}_2)_2]$ complex were optimized without symmetry constraints using the B3P86 functional.^{46,47} The Stuttgart basis set with effective core potential was used for the Ni atom, whereas the 6-31G* basis set was used for all of the other atoms with one additional p polarization function for the proton on the pendant amines. The optimized structures were confirmed by frequency calculations. All of the calculations were carried out with the program Gaussian 09.⁴⁸

■ ASSOCIATED CONTENT

Supporting Information

CIF files giving crystallographic data for $[\text{Ni}(\text{P}^{\text{Cy}}_2\text{N}^{\text{Bn-OMe}}_2)_2](\text{BF}_4)_2$, $[\text{Ni}(\text{P}^{\text{Cy}}_2\text{N}^{\text{Bn-COOMe}}_2)_2](\text{BF}_4)_2$, $[\text{Ni}(\text{P}^{\text{Cy}}_2\text{N}^{\text{Bn-OMe}}_2)_2]$, $[\text{Ni}(\text{P}^{\text{Cy}}_2\text{N}^{\text{Bn}}_2)_2]$, and $[\text{Ni}(\text{P}^{\text{Cy}}_2\text{N}^{\text{Bn-COOMe}}_2)_2]$ and figures and tables giving redox characteristics of $[\text{Ni}(\text{P}^{\text{Cy}}_2\text{N}^{\text{Bn-R}}_2)_2]$ complexes, turnover frequencies for the catalysts with and without the addition of water, ^1H NMR of $\text{P}_2\text{CyN}^{\text{Bn-Ala-OMe}}_2$, scan rate dependence of peak current for the oxidation of the endo-endo isomer of $[\text{Ni}^0(\text{P}^{\text{Cy}}_2\text{N}^{\text{Bn-R}}_2\text{H})_2]^{2+}$, electrocatalysis of $[\text{Ni}(\text{P}^{\text{Cy}}_2\text{N}^{\text{Bn-COOMe}}_2)_2]^+$ in MeCN and $[\text{Ni}(\text{P}^{\text{Cy}}_2\text{N}^{\text{Bn-Phe-OMe}}_2)_2]^{2+}$ in PhCN, electrochemistry of $[\text{Ni}(\text{P}^{\text{Cy}}_2\text{N}^{\text{Bn-OMe}}_2)_2](\text{BF}_4)_2$ with water followed by triethylamine, ^{31}P NMR spectra of $[\text{Ni}(\text{P}^{\text{Cy}}_2\text{N}^{\text{Bn-Phe-OMe}}_2)_2]^{2+}$, ^{31}P – ^{31}P COSY spectra of $[\text{Ni}(\text{P}^{\text{Cy}}_2\text{N}^{\text{Bn-Phe-OMe}}_2)_2]^{2+}$ in CD_3CN taken at -40 °C, and variable-temperature ^{31}P NMR spectroscopy of $[\text{HNi}(\text{P}^{\text{Cy}}_2\text{N}^{\text{Bn-Phe-OMe}}_2)_2]^+$. This material is available free of charge via the Internet at <http://pubs.acs.org>.

■ AUTHOR INFORMATION

Corresponding Author

*E-mail: wendy.shaw@pnnl.gov.

Present Address

[†]Department of Chemistry, Indiana University of Pennsylvania, Indiana, PA.

Notes

The authors declare no competing financial interest.

■ ACKNOWLEDGMENTS

We thank Daniel DuBois for useful discussions. This work was funded by the DOE Office of Science Early Career Research Program through the Office of Basic Energy Sciences (S.L. and W.S.), by the Center for Molecular Electrocatalysis, an Energy Frontier Research Center funded by the U.S. Department of Energy, Office of Science, Office of Basic Energy Sciences (M.-H.H., S.C., S.R., J.A.S.R.), and by the U.S. DOE Basic Energy Sciences, Chemical Sciences, Geoscience and Biosciences Division (A.M.A., A.J., J.C.L.). Computational resources were provided by the National Energy Research Scientific Computing Center (NERSC) at Lawrence Berkeley National Laboratory. Pacific Northwest National Laboratory is operated by Battelle for the U.S. Department of Energy.

■ REFERENCES

- Fontecilla-Camps, J. C.; Volbeda, A.; Cavazza, C.; Nicolet, Y. *Chem. Rev.* **2007**, *107*, 4273.
- Pershad, H. R.; Duff, J. L. C.; Heering, H. A.; Duin, E. C.; Albracht, S. P. J.; Armstrong, F. A. *Biochemistry* **1999**, *38*, 8992.
- Frey, M. *ChemBioChem* **2002**, *3*, 153.
- Cornish, A. J.; Gartner, K.; Yang, H.; Peters, J. W.; Hegg, E. L. *J. Biol. Chem.* **2011**, *286*, 38341.

- (5) Dementin, S.; Burlat, B.; Lacey, A. L. D.; Pardo, A.; Adryanczyk-Perrier, G.; Guigliarelli, B.; Fernandez, V. M.; Rousset, M. *J. Biol. Chem.* **2004**, *279*, 10508.
- (6) Marshall, N. M.; Garner, D. K.; Wilson, T. D.; Gao, Y.-G.; Robinson, H.; Nilges, M. J.; Lu, Y. *Nature* **2009**, *462*, 113.
- (7) Pandey, A. S.; Harris, T. V.; Giles, L. J.; Peters, J. W.; Szilagy, R. K. *J. Am. Chem. Soc.* **2008**, *130*, 4533.
- (8) Rakowski DuBois, M.; DuBois, D. L. *Chem. Soc. Rev.* **2009**, *38*, 62.
- (9) Gloaguen, F.; Rauchfuss, T. B. *Chem. Soc. Rev.* **2009**.
- (10) Wilson, A. D.; Newell, R. H.; McNevin, M. J.; Muckerman, J. T.; Rakowski DuBois, M.; DuBois, D. L. *J. Am. Chem. Soc.* **2006**, *128*, 358.
- (11) Pool, D. H.; DuBois, D. L. *J. Organomet. Chem.* **2009**, *694*, 2858.
- (12) Wilson, A. D.; Shoemaker, R. K.; Miedaner, A.; Muckerman, J. T.; DuBois, D. L.; Rakowski DuBois, M. *Proc. Natl. Acad. Sci. U.S.A.* **2007**, *104*, 6951.
- (13) Yang, J. Y.; Bullock, R. M.; Shaw, W. J.; Twamley, B.; Frazee, K.; Rakowski DuBois, M.; DuBois, D. L. *J. Am. Chem. Soc.* **2009**, *131*, 5935.
- (14) Appel, A. M.; Pool, D. H.; O'Hagan, M.; Shaw, W. J.; Yang, J. Y.; Rakowski DuBois, M.; DuBois, D. L.; Bullock, R. M. *ACS Catal.* **2011**, *1*, 777.
- (15) Helm, M. L.; Stewart, M. P.; Bullock, R. M.; Rakowski DuBois, M.; DuBois, D. L. *Science* **2011**, *333*, 863.
- (16) Wiedner, E. S.; Yang, J. Y.; Chen, S.; Raugei, S.; Dougherty, W. G.; Kassel, W. S.; Helm, M. L.; Bullock, R. M.; Rakowski DuBois, M.; DuBois, D. L. *Organometallics* **2012**, *31*, 144.
- (17) Kilgore, U. J.; Roberts, J. A. S.; Pool, D. H.; Appel, A. M.; Stewart, M. P.; Rakowski DuBois, M.; Dougherty, W. G.; Kassel, W. S.; Bullock, R. M.; DuBois, D. L. *J. Am. Chem. Soc.* **2011**, *133*, 5861.
- (18) Jain, A.; Lense, S.; Linehan, J. C.; Raugei, S.; Cho, H.; DuBois, D. L.; Shaw, W. J. *Inorg. Chem.* **2011**, *50*, 4073.
- (19) Smith, S. E.; Yang, J. Y.; DuBois, D. L.; Bullock, R. M. *Angew. Chem., Int. Ed.* **2012**, *51*, 3152.
- (20) Wiedner, E. S.; Yang, J. Y.; Dougherty, W. G.; Kassel, W. S.; Bullock, R. M.; Rakowski DuBois, M.; DuBois, D. L. *Organometallics* **2010**, *29*, 5390.
- (21) Yang, J. Y.; Chen, S.; Dougherty, W. G.; Kassel, W. S.; Bullock, R. M.; DuBois, D. L.; Raugei, S.; Rousseau, R.; Dupuis, M.; Rakowski DuBois, M. *Chem. Commun.* **2010**, 8618.
- (22) Raugei, S.; Chen, S.; Ho, M.-H.; Ginovska-Pangovska, B.; Rousseau, R. J.; Dupuis, M.; DuBois, D. L.; Bullock, R. M. *Chem. Eur. J.* **2012**, *18*, 6493.
- (23) O'Hagan, M.; Shaw, W. J.; Raugei, S.; Chen, S.; Yang, J. Y.; Kilgore, U. J.; DuBois, D. L.; Bullock, R. M. *J. Am. Chem. Soc.* **2011**, *133*, 14301.
- (24) The spectrum of $[\text{Ni}(\text{P}^{\text{Cy}}_2\text{N}^{\text{Bn-Phe-OMe}}_2\text{H})_2]^{2+}$ contains additional resonances for the hydride at 13.27 ppm (18%) and an unknown impurity at 3.37 ppm at 0 °C (~2%) (Figure 6). The impurity is also present in the $[\text{Ni}(\text{P}^{\text{Cy}}_2\text{N}^{\text{Bn-Phe-OMe}}_2)_2]^{2+}$ used to generate $[\text{Ni}(\text{P}^{\text{Cy}}_2\text{N}^{\text{Bn-Phe-OMe}}_2\text{H})_2]^{2+}$, moves downfield at cooler temperatures, and broadens at higher temperatures. It was investigated by ^{31}P - ^{31}P EXSY at variable temperatures and was not found to exchange with any of the other resonances present.
- (25) Berning, D. E.; Noll, B. C.; DuBois, D. L. *J. Am. Chem. Soc.* **1999**, *121*, 11432.
- (26) Wehman-Ooyevaar, I. C. M.; Grove, D. M.; Kooijman, H.; van der Sluis, P.; Spek, A. L.; van Koten, G. *J. Am. Chem. Soc.* **1992**, *114*, 9916.
- (27) Brammer, L. *Dalton Trans.* **2003**, 3145.
- (28) Brammer, L.; McCann, M. C.; Bullock, R. M.; McMullan, R. K.; Sherwood, P. *Organometallics* **1992**, *11*, 2339.
- (29) Zhao, D.; Ladipo, F. T.; Braddock-Wilking, J.; Brammer, L. *Organometallics* **1996**, *15*, 1441.
- (30) There is a current increase immediately following the Ni(II/I) couple at ~-0.6 V (green), but the current increases linearly with scan rate, suggesting a stoichiometric rather than catalytic process. This wave is tentatively assigned to oxidation of the hydride, $[\text{HNi}(\text{P}^{\text{Cy}}_2\text{N}^{\text{Bn-COOMe}}_2)_2]^+$, which arises from deprotonation of the endo-endo species. Upon addition of water, the irreversible electrochemical event at -0.6 V remains.
- (31) Knorz, P.; Silakov, A.; Foster, C. E.; Armstrong, F. A.; Lubitz, W.; Happe, T. *J. Biol. Chem.* **2012**, *287*, 1489.
- (32) Singleton, M. L.; Bhuvanesh, N.; Reibenspies, J. H.; Darensbourg, M. Y. *Angew. Chem., Int. Ed.* **2008**, *47*, 9492.
- (33) Peters, J. W.; Lanzilotta, W. N.; Lemon, B. J.; Seefeldt, L. C. *Science* **1998**, *282*, 1853.
- (34) Jain, A.; Reback, M. L.; Lindstrom, M. L.; Thogerson, C. E.; Helm, M. L.; Appel, A. M.; Shaw, W. J. *Inorg. Chem.* **2012**, *51*, 6592.
- (35) Heintz, R. A.; Smith, J. A.; Szalay, P. S.; Weisgerber, A.; Dunbar, K. R. *Inorg. Synth.* **2002**, *33*, 75.
- (36) Galan, B. R.; Schöffel, J.; Linehan, J. C.; Seu, C.; Appel, A. M.; Roberts, J. A. S.; Helm, M. L.; Kilgore, U. J.; Yang, J. Y.; DuBois, D. L.; Kubiak, C. P. *J. Am. Chem. Soc.* **2011**, *133*, 12767.
- (37) Wayner, D. D. M.; Parker, V. D. *Acc. Chem. Res.* **1993**, *26*, 287.
- (38) Ellis, W. W.; Raebiger, J. W.; Curtis, C. J.; Bruno, J. W.; DuBois, D. L. *J. Am. Chem. Soc.* **2004**, *126*, 2738.
- (39) Bruker APEX 2, version 2010.3.0; Bruker AXS Inc., Madison, WI, 2009.
- (40) SAINTPlus: Data Reduction and Correction Program; Bruker AXS Inc., Madison, WI, 2004; Vol. 723a.
- (41) SADABS: an Empirical Absorption Correction Program, version 2001/1; Bruker AXS Inc., Madison, WI, 2001.
- (42) ShelDRICK, G. M. SHELXTL: Structure Determination Software Suite, version 6.14; Bruker AXS Inc., Madison, WI, 2004.
- (43) Budzelaar, P. H. M. gNMR 5.0; Adept Scientific, Herts, U.K., 2006.
- (44) QuantumSoft, version 6.2; Fit, P., Ed.; QuantumSoft, Zurich, Switzerland, 2010.
- (45) Braun, S.; Kalinowski, H.-O.; Berger, S. *150 and More Basic NMR Experiments: A Practical Course*; Wiley-VCH: Weinheim, Germany, 1998.
- (46) Perdew, J. P. *Phys. Rev. B* **1986**, *33*, 8822.
- (47) Becke, A. D. *J. Chem. Phys.* **1993**, *98*, 5648.
- (48) Frisch, M. J.; Trucks, G. W.; Schlegel, H. B.; Scuseria, G. E.; Robb, M. A.; Cheeseman, J. R.; Scalmani, G.; Barone, V.; Mennucci, B.; Petersson, G. A.; Nakatsuji, H.; Caricato, M.; Li, X.; Hratchian, H. P.; Izmaylov, A. F.; Bloino, J.; Zheng, G.; Sonnenberg, J. L.; Hada, M.; Ehara, M.; Toyota, K.; Fukuda, R.; Hasegawa, J.; Ishida, M.; Nakajima, T.; Honda, Y.; Kitao, O.; Nakai, H.; Vreven, T.; Montgomery, J. A., Jr.; Peralta, J. E.; Ogliaro, F.; Bearpark, M.; Heyd, J. J.; Brothers, E.; Kudin, K. N.; Staroverov, V. N.; Kobayashi, R.; Normand, J.; Raghavachari, K.; Rendell, A.; Burant, J. C.; Iyengar, S. S.; Tomasi, J.; Cossi, M.; Rega, N.; Millam, J. M.; Klene, M.; Knox, J. E.; Cross, J. B.; Bakken, V.; Adamo, C.; Jaramillo, J.; Gomperts, R.; Stratmann, R. E.; Yazyev, O.; Austin, A. J.; Cammi, R.; Pomelli, C.; Ochterski, J. W.; Martin, R. L.; Morokuma, K.; Zakrzewski, V. G.; Voth, G. A.; Salvador, P.; Dannenberg, J. J.; Dapprich, S.; Daniels, A. D.; Farkas, O.; Foresman, J. B.; Ortiz, J. V.; Cioslowski, J.; Fox, D. J. *Gaussian 09, Revision B.01*; Gaussian, Inc., Wallingford, CT, 2009.